The impact of ROI extraction method for MEG connectivity estimation: practical recommendations for the study of resting state data.

Diandra Brkić , Sara Sommariva , Anna-Lisa Schuler , Annalisa Pascarella , Paolo Belardinelli , Silvia L. Isabella , Giovanni Di Pino , Sara Zago , Giulio Ferrazzi , Javier Rasero , Giorgio Arcara , Daniele Marinazzo , Giovanni Pellegrino

PII: S1053-8119(23)00575-X
DOI: https://doi.org/10.1016/j.neuroimage.2023.120424
Reference: YNIMG 120424

To appear in: *NeuroImage*

Received date: 28 June 2023
Revised date: 18 September 2023
Accepted date: 23 October 2023

Please cite this article as: Diandra Brkić , Sara Sommariva , Anna-Lisa Schuler , Annalisa Pascarella , Paolo Belardinelli , Silvia L. Isabella , Giovanni Di Pino , Sara Zago , Giulio Ferrazzi , Javier Rasero , Giorgio Arcara , Daniele Marinazzo , Giovanni Pellegrino , The impact of ROI extraction method for MEG connectivity estimation: practical recommendations for the study of resting state data., *NeuroImage* (2023), doi: https://doi.org/10.1016/j.neuroimage.2023.120424

Highlights

- Describes how the choice of ROI extraction method affects the estimation of MEG resting state functional connectivity.
- Measures how ROI-based extraction strategies vary across two connectivity measures (ciPLV, PLV) and frequency bands (theta, alpha, beta) in real and simulated data.
- Defines the reliability of extraction methods and how it varies according to the size of the ROI.
- Finally, it provides practical recommendations for future studies and applications.

The impact of ROI extraction method for MEG connectivity estimation: practical recommendations for the study of resting state data.

Diandra Brkić PhD[1], Sara Sommariva PhD[2], Anna-Lisa Schuler PhD[3], Annalisa Pascarella, PhD[4], Paolo Belardinelli PhD[5], Silvia L. Isabella PhD[1,6], Giovanni Di Pino, MD, PhD[6], Sara Zago[1], Giulio Ferrazzi PhD[7], Javier Rasero PhD[8,9], Giorgio Arcara PhD[1], Daniele Marinazzo PhD[10], Giovanni Pellegrino MD, PhD[11]

1. IRCCS San Camillo, Venice, Italy
2. Dipartimento di Matematica, Università di Genova, Genova, Italy
3. Max Planck Institute for Human Cognitive and Brain Sciences, Leipzig, Germany
4. Istituto per le Applicazioni del Calcolo "M. Picone", National Research Council, Rome, Italy
5. CIMeC, University of Trento, Trento, Italy
6. Research Unit of Neurophysiology and Neuroengineering of Human-Technology Interaction (NeXTlab), Università Campus Bio-Medico di Roma, Rome, Italy
7. Philips Healthcare, Milan, Italy
8. CoAx Lab, Carnegie Mellon University, Pittsburgh, USA
9. School of Data Science, University of Virginia, Charlottesville, USA
10. Faculty of Psychology and Educational Sciences, Department of Data Analysis, University of Ghent, Ghent, Belgium
11. Department of Clinical Neurological Sciences, Western University, London, Ontario, Canada

Abstract

Magnetoencephalography and electroencephalography (M/EEG) seed-based connectivity analysis requires the extraction of measures from regions of interest (ROI). M/EEG ROI-derived source activity can be treated in different ways. It is possible, for instance, to average each ROI's time series prior to calculating connectivity measures. Alternatively, one can compute connectivity maps for each element of the ROI prior to dimensionality reduction to obtain a single map. The impact of these different strategies on connectivity results is still unclear.

Here, we address this question within a large MEG resting state cohort (N=113) and within simulated data. We consider 68 ROIs (Desikan-Killiany atlas), two measures of connectivity (phase locking value-PLV, and its imaginary counterpart- ciPLV), and three frequency bands (theta 4-8 Hz, alpha 9-12 Hz, beta 15-30 Hz). We compare four extraction methods: (i) mean, or (ii) PCA of the activity within the seed or ROI *before* computing connectivity, map of the (iii) average, or (iv) maximum connectivity *after* computing connectivity for each element of the seed. Hierarchical clustering is then applied to compare connectivity outputs across multiple strategies, followed by direct contrasts across extraction methods. Finally, the results are validated by using a set of realistic simulations.

We show that ROI-based connectivity maps vary remarkably across strategies in terms of connectivity magnitude and spatial distribution. Dimensionality reduction procedures conducted *after* computing connectivity are more similar to each-other, while PCA *before* approach is the most dissimilar to other approaches. Although differences across methods are consistent across frequency bands, they are influenced by the connectivity metric and ROI size. Greater differences were observed for ciPLV than PLV, and in larger ROIs. Realistic simulations confirmed that *after* aggregation procedures are generally more accurate but have lower specificity (higher rate of false positive connections). Though computationally demanding, *after* dimensionality reduction strategies should be preferred when higher sensitivity is desired. Given the remarkable differences across aggregation procedures, caution is warranted in comparing results across studies applying different methods.

Introduction

Technological advances in neuroimaging over the past three decades have allowed the study of brain connectivity, which has helped to understand the neural basis of healthy cognition and clinical disorders (Schnitzler & Gross, 2005). Today it is well-established that task-based or resting state functional connectivity patterns are markers of efficiency in cognitive processes, while disrupted connectivity patterns may suggest impaired functional brain circuits (Aydin et al., 2020; Baldassarre et al., 2016; Carter et al., 2009; Englot et al., 2015; Hawkins et al., 2020; Pellegrino et al., 2012, 2019; Pellegrino, Mecarelli, et al., 2018; Schuler et al., 2018, 2019; Schuler & Pellegrino, 2021). Among many neuroimaging modalities used to estimate brain connectivity, magnetoencephalography and electroencephalography (M/EEG) are particularly effective because they provide sub-millisecond temporal resolution, direct monitoring of neural activity oscillating across multiple frequencies (Baillet, 2017), acquisitions in a noise-free environment, either while seated, laying down, or walking (Colenbier et al., 2022; Pellegrino et al., 2022; Schuler & Pellegrino, 2021).

While brain functions are spatially distributed, in order to measure connectivity the cerebral cortex is typically divided into parcels, regions of interest (ROI), or seeds, often standardized using atlases (Desikan et al., 2006; Eickhoff et al., 2018; Schaefer et al., 2018). Here, connectivity can be computed considering these regions in a seed-based connectivity fashion. Within this approach measures of functional relationship are typically estimated between one seed and other seeds, or between one seed and the rest of the brain (Betti et al., 2013; Brookes et al., 2011; Siems et al., 2016). When computing seed-based connectivity, the seed can be a

single voxel for volumes, or a vertex for analyses restricted to cortical surfaces, (Brookes et al., 2011; Hipp et al., 2012; Siems et al., 2016). More often seeds include larger regions consisting of multiple elements (voxels or vertices), containing rich and spatially varying information (Kriegeskorte & Bandettini, 2007; Meier et al., 2008). As each element has different connectivity, aggregation procedures are necessary in order to estimate the connectivity of a given region. One of the simplest dimensionality reduction strategies is to consider the average time-course of all elements of the ROI, which is standard procedure in fMRI seed-based connectivity (Basti et al., 2020; Brookes et al., 2011). This is reasonable given the spatial properties of the BOLD signal: large brain regions show some degree of homogeneity in signal and connectivity, allowing thus to extract brain parcellations (Fan et al., 2016; Schaefer et al., 2018; Thirion et al., 2014; Thomas Yeo et al., 2011).

In M/EEG the process of extracting seed-based connectivity is more challenging (Basti et al., 2019, 2020; Capilla et al., 2022; Farahibozorg et al., 2018; Hillebrand et al., 2012; Tait et al., 2021). M/EEG brain signals are not measured directly as the sensors are placed on the scalp (EEG) or several centimeters above (MEG). M/EEG activity is then reconstructed via source imaging, which requires resolving forward and inverse problems (Baillet, 2017; He et al., 2018; Pellegrino, Hedrich, et al., 2016, 2018, 2020). Brain connectivity is then typically measured in the computed source space, as this reduces the bias due to volume conduction and signal leakage, and provides an accurate inference of the topology of brain connectivity (Brunner et al., 2016; Haufe et al., 2013; Hincapié et al., 2017; Lai et al., 2018; Palva et al., 2018; Schaworonkow & Nikulin, 2022; Van de Steen et al., 2019). When the source space is restricted to the cortical surface and the inverse solution is a distributed technique,

source space time-courses are vectors of magnitude and direction for each vertex, that take into account cortical folding (Dale & Sereno, 1993; Hedrich et al., 2017). In other words, time-courses of neighboring vertices have different directions due to the curvature of the cortical folds. In these cases, time-course averaging within the parcel leads to a certain degree of signal cancellation (Ahlfors, Han, Belliveau, et al., 2010; Ahlfors, Han, Lin, et al., 2010; Chowdhury et al., 2018; Hillebrand et al., 2012; Irimia et al., 2012). Alternative approaches exist for extracting a single connectivity pattern from an extended seed, but the effects of these multiple strategies on connectivity patterns remain to be explored (Colclough et al., 2015, 2016; Hillebrand et al., 2012). For instance, it is possible to consider time-course of the first PCA component rather than the average, as a representative of the ROI's time course (Basti et al., 2020; Bruña & Pereda, 2021; Colclough et al., 2015, 2016; Dimitriadis et al., 2018). Another approach involves computing connectivity using time-courses of all seed's elements (voxel or vertex), and then extract the average, PCA, or use multivariate methods (Aydin et al., 2020; Bruña et al., 2023, 2023; Colclough et al., 2016; Dimitriadis et al., 2018; Hillebrand et al., 2012; Palva et al., 2010). A 'multivariate' strategy acknowledges that all elements of the source space and their time-courses carry some useful information, while the aggregation approach such as mean or PCA is the easiest computational choice. Beyond these, a number of more complex procedures (identification of the center of mass, time-series with maximal power, weighted average, etc.) have been proposed (Basti et al., 2019, 2020; Bruña et al., 2023; Chalas et al., 2022; Garcés et al., 2016; Korhonen et al., 2014; Luckhoo et al., 2012).

The purpose of this study is to systematically compare the most common dimensionality reduction strategies to estimate connectivity patterns. Our analyses

were performed using: (i) a large resting state MEG cohort (N=113) where we applied four extraction methods and two connectivity measures, across three frequency bands, using one canonical cortical atlas (Desikan et al., 2006). Furthermore we used realistic simulations in order to compare real data connectivity results with ground truth (simulated data).

In short, this work addresses the following questions: (i) How does the choice of ROI extraction method affect the estimation of resting state functional connectivity? (ii) Are differences between extraction strategies consistent across different connectivity measures (ciPLV, PLV) and frequency bands (theta, alpha, beta)? (iii) Does the reliability of extraction methods vary depending on the size of the ROI? (iv) What are the recommendations for future studies?

1. Methods

2.1 Participants and MEG acquisition

The study was approved by the local Ethics Committee, the Research Ethics Board of the Province of Venice (Italy), and complied with the 1964 Declaration of Helsinki and its later amendments. Every participant provided written and informed consent. All participants were healthy (self-reported) adults, with normal or corrected-to-normal vision, had no history of neuropsychiatric disorders, or brain injuries. Demographic details of the sample of participants included in this analysis are illustrated in Table S1 of the supplementary material. Overall, 84 subjects were included (66 Female, age range 21-58, mean 29 years old). Of these, 23 had two or more resting state sessions, in separate instances, that were treated as independent acquisitions. We analyzed 113 five-minute resting state recordings, acquired using a whole head 275-channel CTF system (VSM MedTech Systems Inc., Coquitlam, BC,

Canada). Participants sat with their eyes closed in a magnetically shielded room. Eye movements (EOG) and cardiac rhythm (ECG) were recorded with bipolar electrodes. The sampling rate was set to 1200 Hz. Prior to the MEG data acquisition, the position of scalp points and anatomical landmarks (nasion, left and right pre-auricular points) were digitized with a 3D Fastrack Digitizer (Polhemus, Colchester, Vermont, USA). The head position within the dewar was tracked using the Continuous Head Localization system.

2.2 MRI data acquisition and analysis

All participants obtained MR images of the head after the MEG session. T1-weighted anatomical images were acquired at 1.5 T with the Achieva Philips scanner (Philips Medical Systems Best, The Netherlands) using the following parameters: TR = 8.3 ms, echo time TE = 4.1 ms, flip angle = 8°, isotropic spatial resolution = 0.87 mm.

2.3 MEG preprocessing and source imaging

All MEG data was analyzed with the Brainstorm MATLAB-based toolbox (Tadel et al., 2011) *(Figure 1)*. First, MRIs were imported and processed with CAT12 (Gaser et al., 2022) for tissue segmentation, cortical reconstruction and cortical labelling. Source space was defined as the cortical mesh extracted with CAT12, and downsampled to 4032 vertices. The ROIs were the 68 cortical regions of the Desikan-Killiany (DK) surface-based atlas (Desikan et al., 2006). MRI-MEG co-registration was performed by fitting a surface between the T1 head shape and the digitized head and fiducial points, acquired prior to the MEG recording, as described in our previous studies (Pellegrino, Machado, et al., 2016). MEG data was preprocessed using: spatial gradient noise cancellation of third order; band-pass filtering [0.3 – 256 Hz] and notch filtering (50, 100, 150 Hz); Signal Space Projection

(SSP) to remove cardiac and eye movement artefacts (Taulu & Simola, 2006; Tesche et al., 1995); downsampling to 128 Hz; data segmentation into 2.5-second epochs; inspection and rejection of epochs affected by residual artefacts or head movement. SSP was chosen for data preprocessing as it is more operator independent, computationally efficient and, based on our experience, leads to better results (Pellegrino, Xu, et al., 2020). Similarly, we chose 2.5 the epoch length according to previous applications by Basti et al. (2020), acknowledging that this could be too short according to other authors (Fraschini et al., 2016). Nevertheless, paired comparisons were applied across aggregation procedures, reducing therefore the impact of this parameter on the outcome of the study. The forward model was computed using overlapping spheres (Pellegrino, Hedrich, et al., 2018). Noise covariance was estimated from a 3-minute empty room MEG recording acquired prior to the experiment. The inverse problem was solved with the weighted minimum norm estimate (wMNE) approach, with dipoles at the source space constrained to be perpendicular to the cortical surface mesh (Brancaccio et al., 2020; Cona et al., 2020; Hämäläinen & Ilmoniemi, 1994; Hincapié et al., 2017; Pellegrino, Maran, et al., 2018).

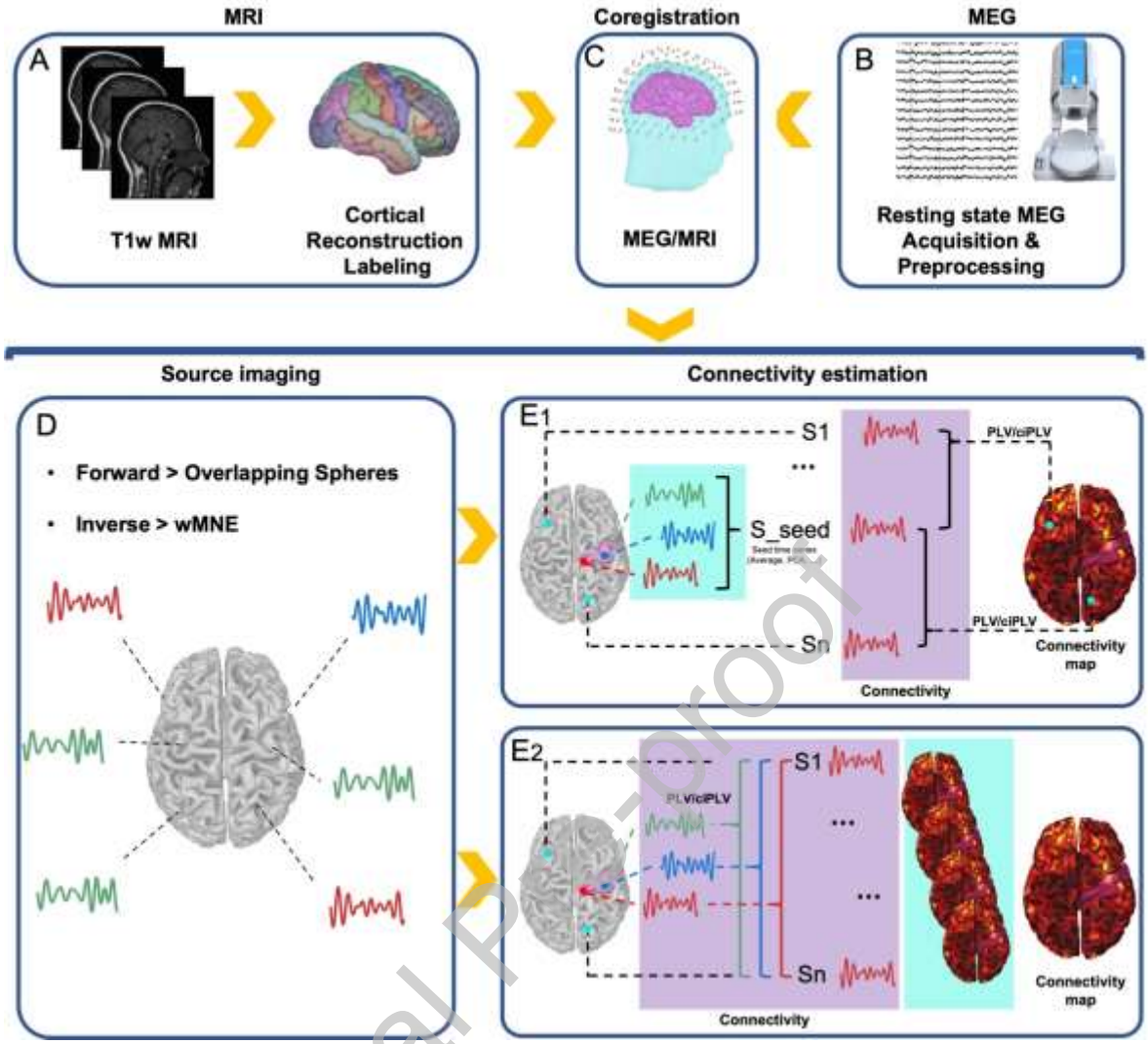

Figure 1. *Analysis pipeline.* **A)** Volumetric T1w MRI was acquired for each participant and processed (segmentation, cortical reconstruction, cortical labeling) with CAT12.The source space corresponded to the cortical surface tasseled into 4000 vertices/nodes. **B**) MEG data was acquired with a 275 CTF system. Data underwent standard preprocessing**. C)** MRI-MEG co-registration was performed with a surface fitting procedure taking into account fiducial points acquired with a Polhemus system **D**) Source imaging was based on an overlapping sphere head model and wMNE inverse solution. This allowed reconstruction of time-series for each of the 4000 nodes of the source space. **E1)** The dimensionality reduction procedure was applied to the time-courses of the vertices/nodes belonging to the ROI (cyan box). Two procedures were considered: (i) the average of the time courses and (ii) the PCA of the time-courses explaining the largest variance. Then the resulting time-course was considered as the seed and pairwise connectivity was estimated with each node/vertex of the source space (purple box). This resulted in a single map representing the connectivity between the ROI and all nodes of the cortex. **E2)** The dimensionality reduction procedure was applied to the connectivity maps computed for each vertex/node of the ROI and the source space (cyan box). The resulting connectivity maps correspond to the number of nodes/vertices of the ROI (purple box). The final output is a single map obtained as an average or maximum of all the maps previously computed.

2.4 Connectivity measures

Connectivity was computed with two measures of phase consistency: the Phase Locking Value (PLV), (Lachaux et al., 1999). and its corrected imaginary counterpart, called corrected imaginary Phase Locking Value (ciPLV), (Bruña & Pereda, 2021). PLV is a measure of phase consistency between two oscillating time series, where higher values represent higher connectivity. More specifically, PLV measures the instantaneous phase difference between two signals based on the assumption that the phase of connected signals are aligned and evolve together (Lachaux et al., 1999; Nolte et al., 2020; Varela et al., 2001). It has been shown how the application of the imaginary part of the complex definition of PLV, ciPLV, is less sensitive than PLV to volume conduction and signal leakage, since it does not consider zero-lag phase alignment (Bruña et al., 2018; Colclough et al., 2016; Palva et al., 2018; Schuler et al., 2022; Tabarelli et al., 2022). The mathematical explanation of differences between PLV and ciPLV are discussed in detail in Nolte et al. (2020). We applied PLV and ciPLV in three canonical frequency bands of interest: theta (5-7Hz), alpha (8-12Hz), and beta (15-29Hz), (Bruña et al., 2018; Nolte et al., 2020). Connectivity was estimated for each frequency band, each of PLV and ciPLV, and between each ROI (68 ROIs of the Desikan-Kiliani atlas) and each element of the source space, resulting in a connectivity map. Each of these maps was represented by an array of 4032 elements, where the value of each element is the connectivity between the ROI and each element (vertex) of the source space. In order to perform group analyses, individual connectivity maps were projected onto a common template (MRI-ICBM152) (Mazziotta et al., 2001) and smoothed with a full width at half maximum of 5mm (Bernal-Rusiel et al., 2010; Brodoehl et al., 2020; Coalson et al., 2018; Hagler et al., 2006; Worsley et al., 2002). Furthermore we considered

coherence as an additional connectivity measure. The results are consistent with ciPLV and PLV outcome, and are described in the supplementary material.

2.5 Dimensionality reduction methods or ROI extraction function

We compared four methods of ROI extraction, illustrated in Figure 1:

a) *Mean before:* mean of the signal within ROI. This function averages all time-courses within the ROI before computing connectivity between the resulting average time-course and the time-course of each element of the source space. This approach is very simple and computationally efficient. As the time-course of adjacent elements of the source space may display a different sign due to the folding of the cortical surface, a flip-sign function is applied before averaging in order to reduce cancellation.

b) *PCA before:* PCA of the signal within the ROI. This method takes the time course of the first component of the PCA decomposition of all the signals within a ROI, before computing the connectivity between the time course of that component and the time course of all elements of the source space.

c) *Mean after*: mean of the connectivity maps computed from all elements of a ROI. Here, dimensionality reduction is applied after the computation of connectivity. A connectivity map is computed for each element of the ROI taking into account the time course of that element and the time-course of all elements of the source space. The final connectivity map corresponds to the average of all the maps belonging to the same ROI.

d) *Max after:* maximum estimate of the connectivity computed for all elements of the ROI. Similar to mean after, but in the Max after function only the maximum value is retained for each element of the resulting connectivity map/vector.

2.6 Clustering analysis

As outlined before, in this study we considered four dimensionality reduction methods and three connectivity measures (ciPLV, PLV, and coherence described in the supplementary material). To assess the similarity across reduction strategies, we conducted a hierarchical clustering analysis based on seed-based connectivity patterns. This analysis was performed separately for the three bands of interest: theta (5-7Hz), alpha (8-12Hz), and beta (15-29Hz). Specifically, for each MEG dataset we initially computed the 8 x 8 similarity matrix (R), where each element resulted from Pearson correlation coefficient computed between connectivity patterns of each joint combination of dimensionality reduction method and connectivity measure. Subsequently, we derived a distance matrix as 1 - <R>, where <R> is the similarity matrix averaged across all MEG datasets. Finally, we applied hierarchical clustering to this distance matrix using the MATLAB linkage function, utilizing the average linkage criterion. We adopted two approaches to this clustering analysis. In the first one, patterns were obtained by concatenating the connectivity maps across all 68 seed regions according to the DK atlas. In the second approach, we simply considered each ROI-specific connectivity map separately. The code for the entire clustering analysis pipeline is openly accessible on Github, (jrasero, 2022/2023)

2.7 Pairwise comparison between scout functions

While the clustering analysis provided an estimate on (dis)similarities across different strategies, and how connectivity maps cluster together, it did not quantify differences across options and their spatial distribution. Therefore, to address the extent to which the use of the four scout functions differed, we performed parametric testing.

Specifically, we applied paired t-testing to compare across all possible combinations of scout functions, for each ROI, frequency band, and connectivity measures (PLV and ciPLV). This analysis was carried out as a post-hoc exploration of the magnitude and spatial distribution of differences across the dimension reduction approaches. We found that the differences across procedures were strong and widespread. In order to make sure that these differences were specific and not caused by a simple offset (i.e. a constant difference), we then repeated the same analysis after normalizing all connectivity maps. Here the maximal connectivity value of each map was set as 100% and all other values were expressed as percentages of the maximum. For these analyses we only report some examples, whereas all comparisons are available as GIfTI at www.hsancamillo.it.

2.8 Simulation of MEG data with known connectivity structure

Applying different ROI-extraction methods to realistic simulations allowed us to depict the properties of each approach in comparison with the 'ground truth'. The MEG forward model was based on individual anatomical data of one of the participants. In line with the real data analysis, the source space was confined to the cortical surface, and the lead field matrix was computed by applying the overlapping sphere model. We simulated neural activity by mimicking five interacting patches (for a schematic representation of the implemented pipeline, refer to Figure 2). For each ROI we randomly drew a point, *v1*, within the ROI and four other vertices, *v2, v3, v4, v5,* outside the selected ROI, with the only constraint being that the distance between each pair of points was at least 5 cm. Around each point *vi*, *i=1,…,5*, we defined a patch *Pi* by considering *vi*'s neighboring source-space elements that were less than 2.5 cm apart. Additionally, as for *P1,* we restricted it to entirely belong to the ROI containing *v1* and we set three possible sizes of the patch, namely (i) all

points with a distance from *v1* lower than 2.5 cm, (ii) 50% of those points by selecting the closest to *v1*, and (iii) only *v1* (Figure 2, Panel A). For each group of patch configurations, we then simulated three time-courses, s1(t), s2(t), s3(t), t=1, …., T, where *T=10000* mimicking about 78 s of neural activity sampled at 128 Hz. To this end, and similar to previous work (Haufe & Ewald, 2019; Sommariva et al., 2019; Vallarino et al., 2021), only alpha band was considered for simulation using three signals following a multivariate autoregressive (MVAR) model of order 5, so that *s1(t)* leads the activity of *s2(t)*, while *s3(t)* is uncorrelated. We only retained stable MVAR models such that (i) for each of the resulting signals the average power spectrum in the alpha band represented at least 40% of the overall average power spectrum, and (ii) the average coherence in the alpha band between *s1(t)* and *s2(t)* was greater than 0.5. Following this, *s1(t)* was assigned to *v1*, *s2(t)* to *v2* and *v4*, and *s3(t)* to *v3* and *v5*. For each patch *Pi* the activity of the remaining points was defined by randomly perturbing the Fourier transform of the time series of the corresponding centre *vi* so as to reach a certain amount of intra-patch coherence (Hincapié et al., 2017). Additionally, a Gaussian window was used to modulate the resulting time-series so that source intensity decreased for increasing distance from *vi* (Figure 2, Panel B). Finally, for each set of patch activities, we computed the magnetic field at sensors and added simulated additive noise according to the random dipole brain noise model PoMAM (Calvetti et al., 2019; de Munck et al., 1992) (Figure 2, Panel C). Hence a total of N=68x3=204 MEG data points were simulated, 68 being the number of ROIs within the DK atlas and 3 being the considered sizes for *P1*.

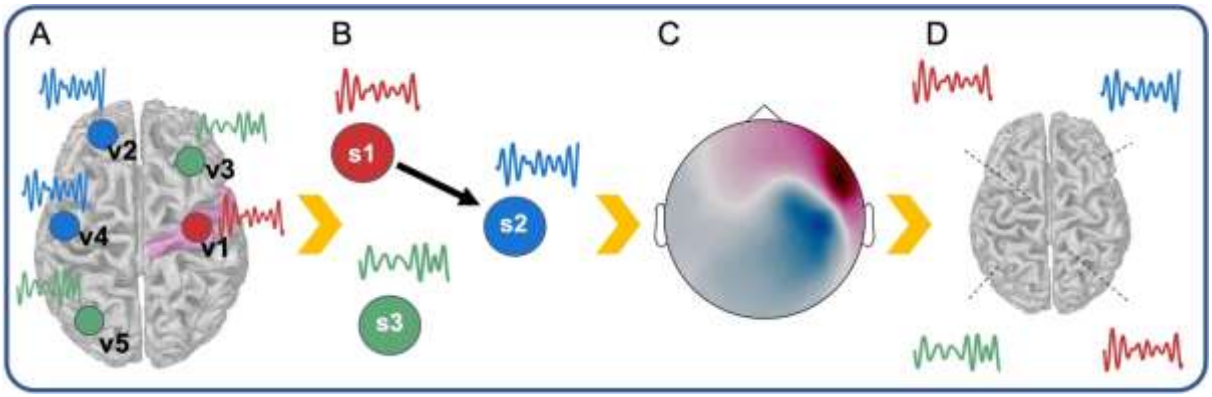

Figure 2. *Simulation Pipeline* **A**) For each ROI we randomly drew a point, v1, within the ROI and four other vertices, v2, v3, v4, v5, outside the selected ROI, with the only constraint that the distance between each pair of points was at least 5 cm. Around each point vi, i=1,…,5, we defined a patch Pi by considering vi's neighbouring source-space elements that were less than 2.5 cm apart. We set three possible sizes of the patch, namely (i) all points with a distance from v1 lower than 2.5cm, (ii) 50% of those points by selecting the closest to v1, and (iii) only v1**. B)** For each group of patch configurations, we simulated three time-courses, s1(t), s2(t), s3(t) so that s1(t) leads the activity of s2(t), while s3(t) is uncorrelated. s1(t) was assigned to v1, s2(t) to v2 and v4, and s3(t) to v3 and v5. For each patch Pi the activity of the remaining points was defined by randomly perturbing the Fourier transform of the time series of the corresponding centre vi so as to reach a certain amount of intra-patch coherence**. C)** for each set of patch activities, we computed the magnetic field at sensors and added simulated additive noise according to the random dipole brain noise model PoMAM. **D)** A total of N=204 MEG data points were simulated. Source space signals were reconstructed using a similar procedure as was used for real data.

2.9 Connectivity estimate and evaluation criteria

As with the experimental MEG data, neural activity was estimated from the simulated MEG data by using the wMNE inverse solution, while connectivity was quantified from the source space estimated time-courses through PLV and ciPLV. Specifically, for each of the 204 simulated signals and for the two connectivity measures, we estimated cortical connectivity maps by considering as seed the ROI containing *v1*. The four ROI extraction methods, i.e. Mean before, PCA before, Mean after, and Max after, were used to quantify the connectivity between this ROI and all 4002 other elements of the source space (Figure 2, Panel D).

To evaluate the results, we exploited the fact that, when P1 only includes *v1*, a ground truth can be defined by computing the values of PLV and ciPLV between *s1* and the activity in all the other points of the source space. Hence for these simulated MEG data, connectivity metrics, and scout function, we computed Pearson correlation coefficient between the estimated cortical connectivity maps and the corresponding ground truth. On the other hand, when *P1* includes more than one element, defining a ground truth is not straightforward. For this reason, we also evaluated the accuracy of the estimated connectivity maps by computing true and false positive rates (TPR and FPR, respectively). To this end, we fixed one hundred thresholds uniformly distributed between 0 and 1 (alpha). Then for each of the simulated MEG data points, for each of the four scout functions and for both connectivity measures, we applied a normalization procedure by rescaling each map with its maximum value. Thereafter, for each map, for every alpha value of the threshold, we defined:

$$TPR\,(alpha) = \frac{TP(alpha)}{P} \quad \text{and} \quad FPR\,(alpha) = \frac{FP(alpha)}{N}$$

where:

- *P* and *N* are the number of positive and negative, respectively. *P* counts the source-space points truly connected with *v1*, i.e. the nodes within *P2* and *P4* in our simulations, while *N* is the number of the remaining source-space points without considering the nodes of the patch *P1* centered in *v1*.
- *TP(alpha)* is the number of true positives, i.e. points of the source space truly connected to *v1* where the normalized reconstructed connectivity value (either PLV or ciPLV) exceeded the threshold alpha.

- *FP(alpha)* is the number of false positives, which are points not truly correlated with *v1* but where the normalized reconstructed connectivity still exceeded alpha.

Finally, results in terms of True/False positive rate were summarized by computing the corresponding *Receiver Operating Characteristic (ROC)* curve and the associated *Area Under the Curve (AUC)*.

2. Results

This section describes results that focus on PLV and ciPLV, as connectivity measures. The results for coherence can be found in the supplementary material.

3.1 Hierarchical Clustering

The results of the hierarchical clustering are summarized in *Figure 3*. This analysis showed similar patterns of similarity-dissimilarity across frequency bands *(Figure 3, rows)* and the two connectivity measures of interest (PLV and ciPLV).

Similarity map was overall higher and distances overall lower for PLV than ciPLV *(Figure 3, Left and right columns).* Across all frequency bands, PLV and ciPLV maps clustered together within connectivity measures *(Figure 3, middle column)*. The relative distances across extraction methods also clustered consistently together within connectivity measure (*Figure 3, middle column*). We observed that *Max after* and *Mean after* were the two most similar extraction procedures, and as such clustered together under all circumstances, all frequency bands and both connectivity measures (*Figure 3, middle column*). *Max after* and *Mean after* were relatively close to *Mean before*, and clustered together, whereas *PCA before* had higher distance from all other approaches *(Figure3, middle and right columns)*.

The right column in *Figure 3* illustrates that *Mean after* and *Max after* had the lowest distance, followed by *Before-Mean after*.

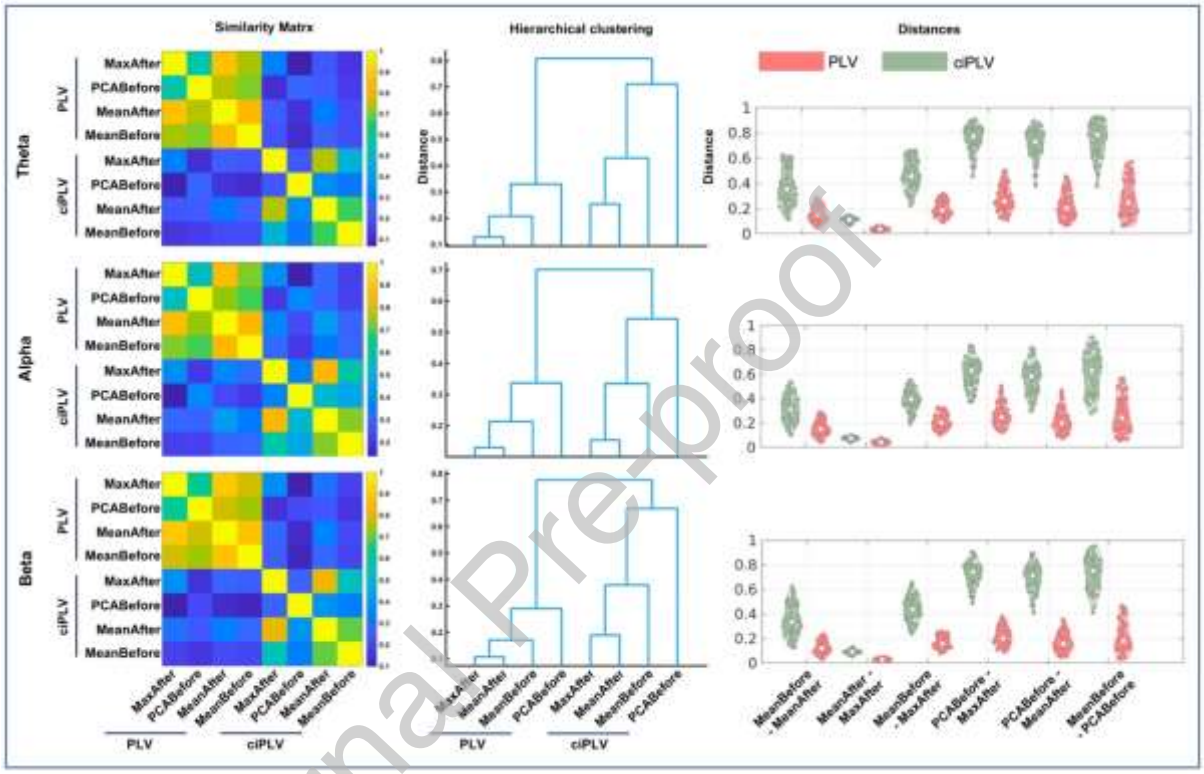

Figure 3. *Hierarchical Clustering.* The figure shows the clustering results by *frequency band* (*rows*). **Left:** similarity matrices. The color scale indicates the similarity of connectivity maps across connectivity measures (*PLV and ciPLV*) and extraction methods (*Max after, PCA before, Mean after, Before*). **Middle:** Dendrograms with distances across aggregation procedures. **Right**: Distances across extraction procedures by connectivity measure (*PLV* and *ciPLV*). Map similarity was overall higher and distances overall lower for *PLV* than *ciPLV (Left and right columns). PLV* and *ciPLV* maps cluster together within connectivity measures for all frequency bands *(middle column)*. The relative distances across extraction methods also clustered consistently together within connectivity measure (*PLV* and *ciPLV*, *middle column*). The most similar extraction procedures were *Max after* and *Mean after*, which were closely clustered, followed by Before, which clustered with both *Max after* and *Mean after*. *PCA before* was most distant from all other approaches, as seen in both *middle and right columns*. The right column shows that *Mean after* and *Max after* had the lowest distance, followed by *Before-Mean after*.

The topographical distribution of the distances across extraction methods is highlighted in *Figure 4*, left panel. The lowest distances were found in the deep regions especially of the midline, for all frequency bands. The higher distances were found especially in the convexity, over the fronto-central regions, and parietal regions (*Figure 4*).

There was a significant and positive relationship between the size of the region and the average distance across extraction methods (*Figure 4, right),* with Pearson correlation coefficient ranging between $r>0.7$ and $p<0.001$, across frequency bands and connectivity measures.

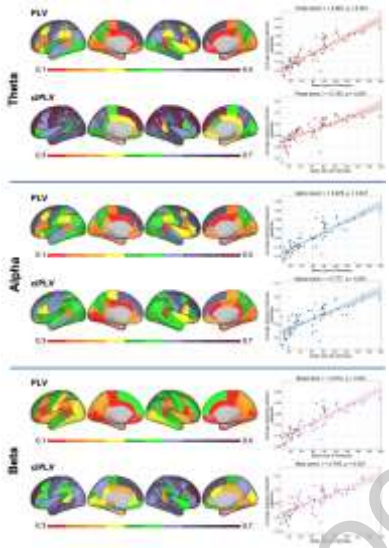

Figure 4. Topographical distribution of average distances by frequency band (rows) and relationship between the size of the parcel and average distances. **Left:** The lowest distances were found in deep regions, especially of the midline, across connectivity measures and frequency bands. The higher distances were found especially in the convexity, over the fronto-central regions, and parietal regions. **Right:** There was a significant positive relationship between the size of the region and the average distance across extraction methods.

3.2 Paired comparisons

The cluster analysis provides a pattern of similarities but does not provide an immediate estimation of the magnitude and spatial distribution of differences across strategies. Therefore, we followed up on clustering analysis by estimating how connectivity changed by paired comparisons between the four strategies under investigation. Specifically, for each connectivity measure and within each frequency band, we compared: i) *Mean before* vs *PCA before*; ii) *Mean before* vs *Mean after*; iii) *Mean before* vs *Max after*; iv) *PCA before* vs *Mean after*; v) *PCA Before* vs *Max after*; vi) and *Mean after* vs *Max after*. For each of these comparisons, we computed

t-maps as a representation of normalized differences between each pair of strategies (illustrated in Supplementary Figure S3). ciPLV connectivity maps computed showed differences as high as 40 t-values, with magnitude and direction (positive/negative) were consistent across frequency bands (alpha, beta, theta). Similar patterns were observed for PLV.

3.3 Simulations results

3.3.1 Correlation between true (simulated) and estimated maps

The results of the correlation between connectivity estimated and true (simulated) when the patch P1 contains only its center v1 are summarized in *Figure 5*. For both PLV and ciPLV and for all aggregation procedures the correlation coefficients are rather low *(< 0.15, Figure 5, upper row)*. This result is expected, as the simulated map does not contain any activity for a large portion of the cortical surface, whereas the estimated map may contain some activity over the entire surface as a result of signal leakage associated with the inverse solution. Similarly PLV did provide lower values for this correlation, being more sensitive to source leakage than ciPLV. Finally, negative values of the correlation coefficient correspond to data where the value of connectivity estimated in the patches that were uncorrelated with v1, namely P3 and P5, was on average higher than the value of connectivity estimated in the correlated patches, namely P2 and P4. In this scenario, the aggregation approaches applied after computing connectivity generally perform better. When applying PLV, the correlation between estimated and simulated connectivity is significantly higher (better) for *Mean after* as compared to *Mean before* and *PCA before* (*Wilcoxon signed-rank, p<0.05 consistently*). When applying ciPLV Max after performs slightly

but significantly better than all other approaches (*Max after vs PCA before W=1761, p=0.003; Max after vs Mean before W=1897, p=0.0001; Max after vs Mean after W=1690, p=0.02*) and Mean after performs slightly better than Mean before (*W =1793, p=0.002*).

We repeated the correlation analysis by restricting true and estimated connectivity maps to the points pertaining to the four active patches, namely P2-P5 (*Figure 5, bottom row*). In this scenario, correlation coefficients are remarkably higher, especially for ciPLV. The aggregation approaches applied after computing connectivity remained slightly better, especially for ciPLV. The correlation coefficient of both ciPLV Mean after and ciPLV Max after, were significantly higher than ciPLV Mean before and ciPLV PCA before (*Mean after vs Mean before W=1944, p=3*10^-5; Mean after vs PCA before W=2023, p=2.5*10^-6; Max after vs Mean before W=2043, p=1.3*10^-6; Max after vs PCA before W=2018, p=2.9*10^-6*). Note that no significant difference was observed comparing ciPLV Max after and Mean after. Interestingly, in this scenario the correlation coefficient was less stable for PLV, with high levels of variance depending on the aggregation procedure. Here the only significant difference was in the comparison between Mean after which was higher than Max after *(W=1835 p=6*10^-4).*

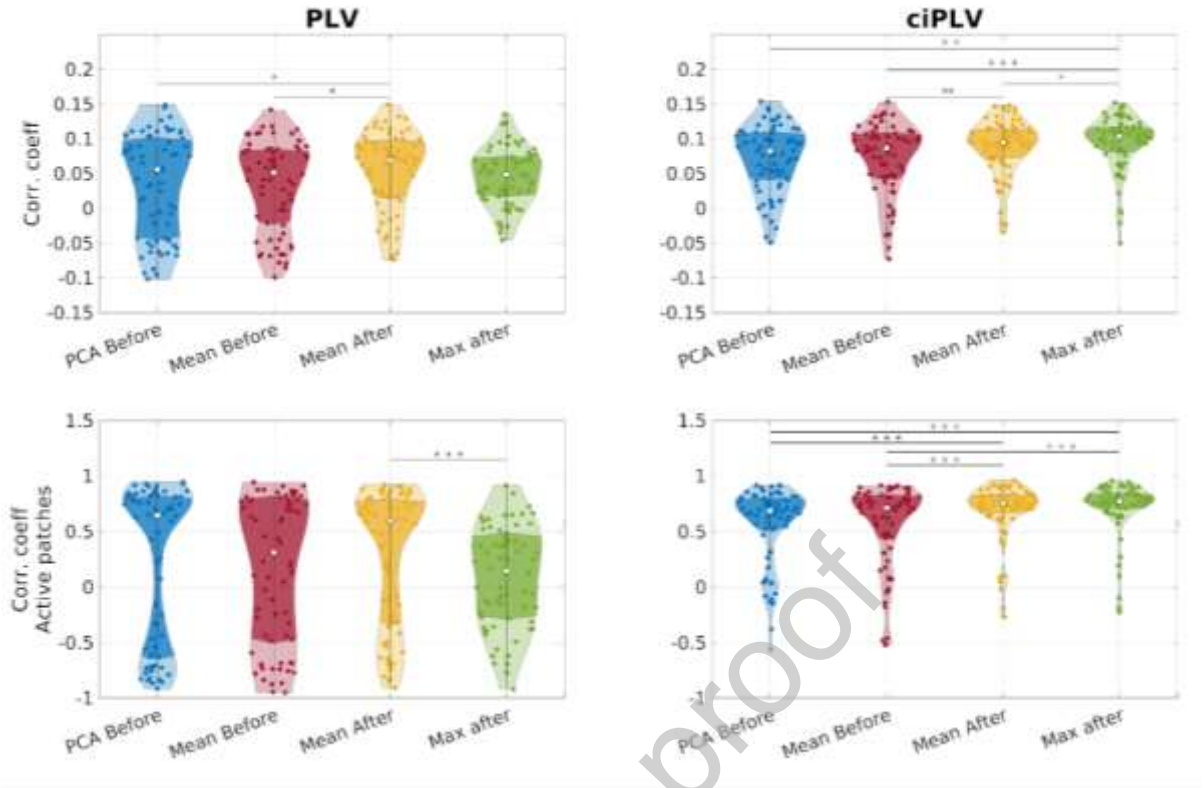

Figure 5. Pearson correlation coefficient between true (simulated) and estimated connectivity maps across 68 simulated neural activity sources such that P1 contains only the center v1. **Upper row, left**. PLV correlation coefficients of maps defined in the entire source-space. *Mean after* performed better than *Mean before* and *PCA before***. Upper row, right** ciPLV map correlation coefficients defined for the entire source-space. *Max after* performed significantly better than all other aggregation approaches. *Mean after* performed significantly better than *Mean before*. **Lower row, left** PLV correlation coefficients of maps containing only P2-P5. The distribution of correlation coefficients was remarkably variable across aggregation procedures. *Mean after* performed significantly better than *Max after.* **Lower row, right** ciPLV correlation coefficients of maps containing only P2-P5. Both *Mean after* and *Max after* performed significantly better than *Mean before* and *PCA before.* Note, in the violin plots, white dots depict median values. Darker colors correspond to the interquartile range. $*$ $p < 0.05$, $**$ $p < 0.005$, $***$ $p < 0.0005$.

3.3.2 Accuracy of estimated maps (true and false positive rates)

The analysis of False (FPR) and True (TPR) Positive rates provides more insight in interpreting results from the clustering analysis performed on the experimental resting-state data. *FPR(alpha)* and *TPR(alpha)* are reported in *Figure 6*. This analysis is focused on the case of P1 only containing the center v1, which is a scenario analogous to the one described in the previous paragraph .

For both PLV and ciPLV the two *before* procedures *(Mean before and PCA before)* show higher specificity, while the two *after* procedures *(Mean after and Max after)* show higher sensitivity. Indeed, *PCA before and Mean before* show a lower false positive with the tradeoff of identifying fewer true connections. In other words, these aggregation procedures seem to be more conservative. This means that the reconstructed connections most likely identify truly connected sources, at the expense of weak connections which may be lost when these aggregation procedures are used. Vice versa, *Mean after* and *Max after* show a higher value of both true and false positive rates. This seems to suggest that weak connections may be retrieved at the expense of retaining spurious connectivity. Also note that for both ciPLV and PLV the FPR and TPR curves are very similar and overlap for most of the alpha range.

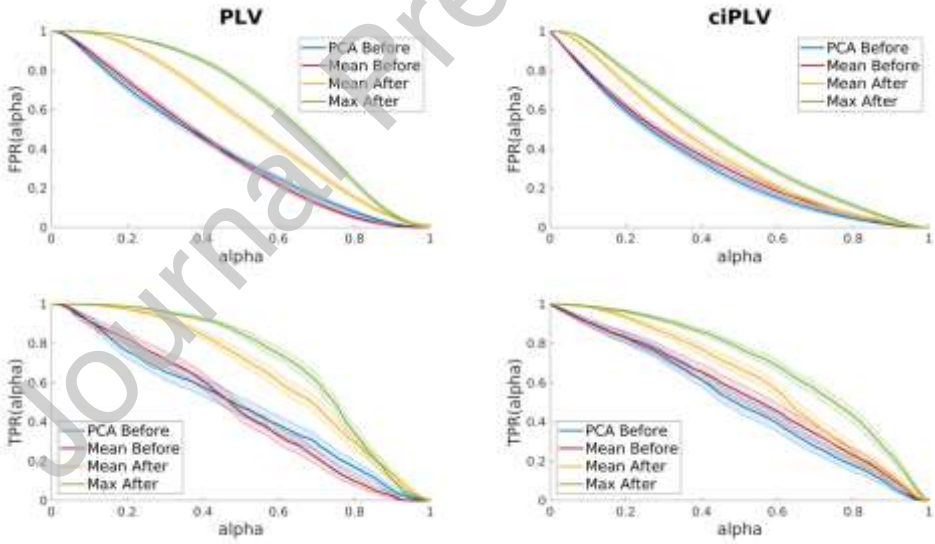

Figure 6. False Positive Rates (*upper row*) and True Positive Rates (*lower row*) models of the two connectivity measures (PLV -*left*- and ciPLV -*right*-) extracted via the four different aggregation procedures. Plots show mean and standard error of the mean across 68 simulated neural activity so that P1 only contains the centre v1. Results concerning different sizes of P1 can be found in the supplementary material.

Similar results are obtained when varying the size of PI *(supplementary material)*. Although the differences across aggregation procedures can vary, Max after and Mean after typically show a higher rate of FPR and TPR.

The comparison of the AUC for all conditions under investigation *(Figure 7)* shows a significantly higher value for Max after and Mean after for ciPLV when only the centre of P1 is considered (*Mean after vs Mean before W=1792, p=0.002; Mean after vs PCA before W=1830, p=7*10^-4; Max after vs Mean before W=1914, p=7.15*10^5; Max after vs PCA before W=1907, p=8.75*10^-5*). The distribution of the AUC values is similar for the four ROI-extraction methods when all points of the patch P1 are considered. With respect to the PLV metric, the distribution of AUC values is significantly higher for Mean after regardless of the dimension of the P1 patch (*Mean after vs PCA before W=1656, p=0.037 when P1 containing only v1; Mean after vs Max after W=2068, p=5.4*10^-7 when P1 contains half points; Mean after vs Max after W=1957, p=2*10^-5 when P1 contains all voxels*).

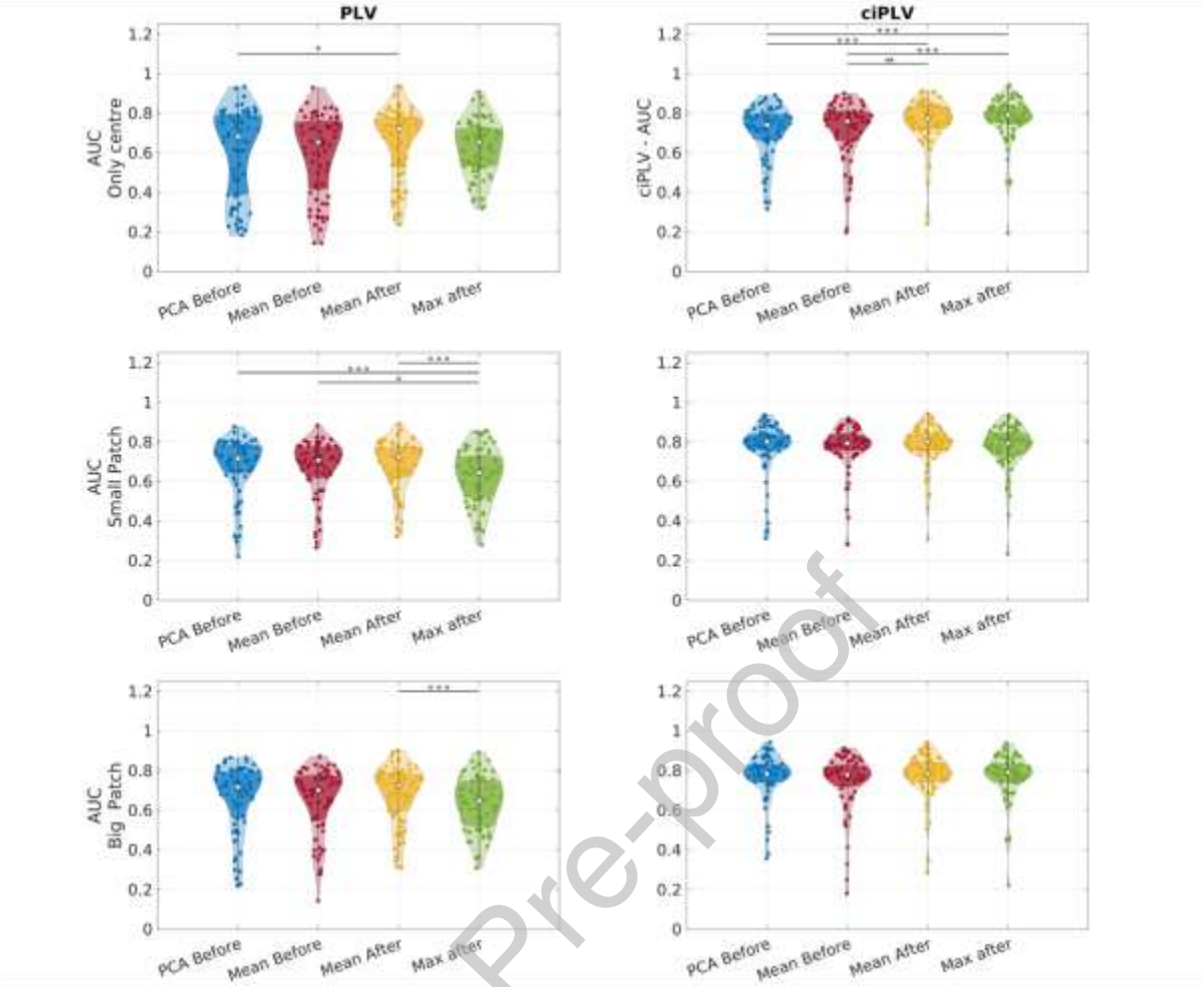

Figure 7. Distribution of the AUC values across the simulated MEG data when the patch P1 contains all the points that are less than 2.5cm apart from v1 (third row), half of such points (*second row*), only its centre v1 (*first row*). Left column shows results concerning PLV while right column refers to ciPLV.

3. Discussion

The findings of this study indicate that the choice of dimensionality reduction method has a significant impact on the resulting connectivity outcomes. These results were observed in both resting state data and realistic simulations. Interestingly, the choice of extraction method resulted in considerable differences in both the magnitude and distribution of connectivity. More specifically via cluster analysis, we observed that the aggregation procedures applied after computing connectivity yielded more consistent results. This was observed for both in-vivo and simulated data.

The *after* approaches are computationally demanding, but allow for the integration of information from all elements of a given parcel, thus providing a more comprehensive connectivity estimation (Aydin et al., 2020; Bruña et al., 2023, 2023; Colclough et al., 2016; Hillebrand et al., 2012; Palva et al., 2010).

The results of the clustering analysis also revealed that the *Mean before* method produced connectivity maps that were similar to those generated by the *after* strategies. On the other hand, *PCA before* method showed results that were markedly dissimilar from all other approaches. While cluster analysis alone may suggest that the *Max after*, *Mean after*, *Mean before* and *Mean after* methods produce similar results, it is important to note that this approach is based on correlations across maps and does not provide enough information about the actual topographical distances. Therefore to gain a better understanding, we conducted pairwise analysis of connectivity maps generated by different extraction strategies. Our results revealed that the most similar maps differed by a magnitude of 40+ t-values, indicating that even minor variations in method choice lead to significant differences in connectivity outcomes (*Supplementary Figure S3*). We also ruled out the possibility that these differences were due to an offset of connectivity values by directly contrasting normalized maps, where each connectivity value was rescaled against the maximum. Here we observed important and widespread differences in connectivity outcomes. Hence, caution is warranted when comparing connectivity patterns between studies that employ different extraction strategies, as even small variations in method can lead to significant discrepancies.

Our analysis also shed light on some of the factors that may influence the effect of extraction method on connectivity outcomes. Specifically, we observed that similarity across extraction methods was higher for *PLV* as compared to *ciPLV* (*Figure 3*).

Both connectivity measures employed in this study are based on phase synchrony across time series. However, *ciPLV* is insensitive to Lag=0 connectivity and as such, is less susceptible to volume conduction and spatial leakage (Bruña et al., 2018; Bruña & Pereda, 2021; Colclough et al., 2016; Lachaux et al., 1999; Nolte et al., 2020; Palva et al., 2018; Schuler et al., 2022; Tabarelli et al., 2022; Varela et al., 2001). Therefore, the resulting connectivity maps are typically less smooth, possibly explaining why similarities across extraction methods is lower than for *PLV (Figure 3)*. On the other hand, our results also highlight that other connectivity measures may exhibit varying levels of robustness to the extraction methods. We observed no relevant differences across frequency bands, although the spatial distribution of the distances shows a trend towards greater differences for lower frequencies (*Figure 3 and 4*). Low frequency activity recorded from the scalp typically originates from large populations of neurons or from large distribution of high frequency activity (Pellegrino et al., 2017; Tao et al., 2007). It is then possible that differences in aggregation methods are more pronounced when the underlying generators span widespread brain areas. This idea is supported by the significant positive linear relationship we observed between the size of the parcel (expressed in number of vertices) and the average difference across extraction methods and frequency bands (*Figure 3*). Given the effect of the parcel size, one could opt for cortical parcellations with smaller parcels than the ones used here, and of similar size if the objective is to minimize the bias of aggregation procedures across parcels. *Figure 4* provides some insight into the topographical distribution of the differences. Smaller differences are more often observed in deep regions especially of the midline. MEG spatial sampling is not homogeneous across the cortical surface, and the reconstruction of source signal in deep, basal, and midline regions is not always accurate in MEG (Ahlfors,

Han, Belliveau, et al., 2010; Gavaret et al., 2014; Huiskamp et al., 2010). It is plausible that the estimation of cortical connectivity was less refined in those areas, and the differences across methods were smaller.

Alternatively, the distribution of rhythms across the cortical surface with more alpha activity in the posterior quadrant, more theta activity in the temporal lobes, and faster activity in the range of beta band in the central regions may have played a role in determining this spatial distribution. Overall, these findings suggest that the choice of extraction method may have a greater impact on connectivity measures in lower frequency bands and in regions that are more challenging to capture with MEG.

Furthermore group comparisons were defined based on the aggregation procedure. The magnitude of the differences between aggregation procedures is large enough that effects could be appreciated at single subject level. Although the contribution of individual differences was not systematically assessed in this instance, we have provided open access to individual connectivity maps, for future studies to explore.

While MEG resting-state data allowed us to identify relative differences across extraction methods, it was challenging to determine which method was more accurate. This prompted us to conduct realistic simulations to gain a more comprehensive understanding of the performance of different methods (Grova et al., 2016; Hincapié et al., 2017; Machado et al., 2018; Sommariva et al., 2019).

Our simulations confirmed that aggregation procedures performed after the computation of connectivity may provide more accurate results. The correlation coefficient between simulated and estimated maps of connectivity was significantly higher for *Mean after* for *PLV*, and for *Mean after* and *Max after* for *ciPLV*. To better understand the performance of different methods, we estimated true and false positive connections captured by applying different aggregation methods. This

analysis revealed that *Mean after* and *Max after* captured a larger number of true connections, but also a larger number of false positives. In other words, *Mean after* and *Max after* showed higher sensitivity for connectivity, but lower specificity.

As for the AUC values, we found that there were differences between *PLV* and *ciPLV*. For *ciPLV*, *Mean after* and *Max after* performed better (with higher AUC) when only the center of the patch was considered, while for *PLV*, *Mean after* had the highest AUC regardless of the parcel size. While different strategies may be more or less appropriate depending on the specific scenario, and it may be difficult to determine which aggregation method performs best in real-world situations. Our results suggest that *Mean after* and *Max after* may be preferable, however at the expense of longer computation time and higher rates of false positives. In addition, while PCA provided maps that were very different from all other extraction methods in real data, simulated data showed similar behaviour to *Mean before*. Overall, we believe it is reasonable to choose *Mean before* when higher specificity and shorter computation time are desired, and *Mean after* when greater sensitivity is prioritised.

The effects of extraction methods on connectivity analysis have been extensively studied in the fMRI field. Previous research has shown that dimensionality reduction at the ROI level can result in the loss of important information (Basti et al., 2019). As an alternative it has been proposed that multi-dimensional connectivity methods could provide more accurate results [Geerligs et al., (2016); for a recent review see Basti et al., (2020)]. The application of dimensionality reduction strategies at the seed level, to obtain a single time-course, is recommended only in the case of homogeneous ROIs. This is rare in M/EEG signal due to cortical folding that often results in opposite directions for reconstructed source space time-courses. Many advanced multivariate approaches that integrate the computation of connectivity and

the extraction of unique patterns of relationship among brain regions have been developed (Basti et al., 2018; Ewald et al., 2012). A recent MEG simulation study compared standard procedures based on the identification of a representative time-course or ROI (average, centroid, largest power, first PCA component, and first Kosambi-Hilbert torsion component) versus the multivariate approach, and concluded that the latter is remarkably better (Bruña & Pereda, 2021). Another study compared three approaches to extract ROI-based time courses (centroid, first PCA component, average), and two multivariate approaches, namely the average of the pairwise connectivities across all elements of the ROIs (corresponding to the *Mean after* of our study) and the root-mean-square (RMS) of all pairwise connectivity in an EEG-MEG study (Bruña et al., 2023). The results showed that multivariate procedures (*Mean after* and RMS post) performed better based on the concordance between EEG and MEG connectivity. Given that no ground truth was available in this study, it cannot be ruled out that some of the results are driven by inherent differences of EEG and MEG. Despite the development of new multivariate approaches, the majority of M/EEG researchers continue to rely on default approaches built in among most commonly used toolboxes for connectivity analyses (i.e., Brainstorm, Fieldtrip, MNE python), (Gramfort et al., 2014; Oostenveld et al., 2011; Tadel et al., 2011). Within these toolboxes, the most used extraction strategy is the average time course of the ROI. The use of PCA for dimensionality reduction has received conflicting evaluations. Some studies suggest that PCA may perform better than averaging the seed signal in cases where the signal is better captured by some voxels than others (Basti et al., 2020). Other studies suggest that PCA may be biased towards weighting more low frequencies at the expense of high frequencies (Chalas et al., 2022). A recent simulation study demonstrated that PCA appears to

be the best technique, particularly when a fixed number of components is chosen across areas. However, this is only true when PCA is coupled with other optimal pieces of the pipeline, including specific inverse solutions and connectivity measures (Pellegrini et al., 2022). Furthermore a MEG study in clinical and control populations revealed that PCA is outperformed by the centroid of the ROI (Dimitriadis et al., 2018) . This means that the choice of the aggregation procedure matters in healthy subjects as well as in patient populations. Lastly, it is important to underlie that the application of PCA entails (arbitrary) choices for several parameters. For instance, several rules regarding the number and properties of the components to retain can be applied. Or whether to apply PCA to individual/single segments of data or to all data at once. The investigation of all possible combinations was beyond the scope of this study. Here we used the implementation available in Brainstorm in 2022 and warn the reader that, albeit computationally efficient, this approach has its own limitations.

Limitations

There are several limitations to the current study. First, the results might not be generalizable to all possible strategies, which was beyond the scope of this study. The focus of the current study was on a set of common and practical scenarios. As such, the effect of flip sign was not investigated for the procedures of aggregation prior to computing connectivity, even though this is a popular approach to limit cancellation effects (Ahlfors, Han, Belliveau, et al., 2010; Lai et al., 2018). The influence of flip sign on the estimation of connectivity remains unclear and requires further systematic investigation.

Furthermore in the analysis of both experimental and simulated data, for each ROI we generated a connectivity map of size 1 x N representing connection strength between that ROI and all the points of the source space. This representation was chosen because it allowed a more intuitive visualization and interpretation of the results. It also made possible to investigate the impact of ROI features such as size. Moreover, in the simulations this representation allowed a straightforward definition of the ground truth connectivity pattern without involving aggregation procedures that could have biased the final results. Additional care is required in studies where additional reduction strategies are performed. For instance when applying the aggregation procedures at both seed and target levels, to obtain connectivity matrices of size NxN (being N the number of ROIs).

Another limitation is that the study only focused on resting-state data. While many studies have shown that some patterns of connectivity remain consistent between rest and tasks, recent literature suggests that individual variations should be considered (Colenbier et al., 2023). Therefore, the generalizability of the results to task-based data may be limited.

Here we obtained consistent results across different connectivity measures (ciPLV, PLV, and Coherence). We believe that this study is a strong proof of principle showing the relevance of the aggregation procedures in studying resting state connectivity. Nevertheless, the scope of this study was limited to three connectivity measures. It remains to be determined the extent to which these results depend on the choice of connectivity measures, that go beyond phase or amplitude based metrics. Some of the most popular estimation methods, such as Temporal Granger, Frequency Granger (Cekic et al., 2018), Transfer Entropy (Vicente et al., 2011),

Partial Directed Coherence (Astolfi et al., 2006), etc. are not considered here, and should be investigated in future studies.

Lastly the simulation presented in this work rely on MVAR model, a linear model often used to simulate neural signals with realistic and possibly time-varying spectra (Chella et al., 2019; Haufe et al., 2013; Haufe & Ewald, 2019; Pagnotta & Plomp, 2018; Sommariva et al., 2019; Vallarino et al., 2021; West et al., 2020). Future work will be devoted to extending our results to more sophisticated models, such as spiking neurons or neural masses (Garofalo et al., 2009; Orlandi et al., 2014; Ricci et al., 2021; Ursino et al., 2020; Wang et al., 2014; Wendling et al., 2002, 2009), where excitatory and inhibitory populations produce oscillations in feedback with different synaptic dynamics, and the corresponding connectivity involves delays and glutamatergic/GABAergic dynamics. Ideally future analyses will include intracranial EEG data too. This is planned future direction, in order to provide a more comprehensive evaluation of the different aggregation procedures.

Conclusions

The current study highlights the critical importance of the aggregation procedures in determining accurate connectivity estimations, in both real and simulated data. The choice of the extraction method has a great impact on the connectivity output. Differences are higher for ciPLV than PLV, with a similar pattern across frequency bands. Further, larger is the ROI the higher is the difference across connectivity outputs obtained with different strategies. Overall to obtain higher accuracy (higher sensitivity at the expense of lower specificity), *after* aggregation procedures (*Mean after*) are recommended in connectivity analyses, even though they are computationally demanding. Given the significant differences across aggregation

methods, it is essential to exercise caution when comparing studies that employ different methods.

Lastly, as this study focused on resting-state data, further research is required to determine similar comparisons for task-based, clinical populations and any other groupwise comparisons.

Disclosure of competing interest

Declarations of interest: none.

References

Ahlfors, S. P., Han, J., Belliveau, J. W., & Hämäläinen, M. S. (2010). Sensitivity of MEG and EEG to source orientation. *Brain Topography*, *23*(3), 227–232. https://doi.org/10.1007/s10548-010-0154-x

Ahlfors, S. P., Han, J., Lin, F.-H., Witzel, T., Belliveau, J. W., Hämäläinen, M. S., & Halgren, E. (2010). Cancellation of EEG and MEG signals generated by extended and distributed sources. *Human Brain Mapping*, *31*(1), 140–149. https://doi.org/10.1002/hbm.20851

Astolfi, L., Cincotti, F., Mattia, D., Marciani, M. G., Baccala, L. A., Fallani, F. D. V., Salinari, S., Ursino, M., Zavaglia, M., & Babiloni, F. (2006). Assessing cortical functional connectivity by partial directed coherence: Simulations and application to real data. *IEEE Transactions on Biomedical Engineering*, *53*(9), 1802–1812. https://doi.org/10.1109/TBME.2006.873692

Aydin, Ü., Pellegrino, G., Ali, O. B. K., Abdallah, C., Dubeau, F., Lina, J.-M., Kobayashi, E., & Grova, C. (2020). Magnetoencephalography resting state connectivity patterns as indicatives of surgical outcome in epilepsy patients. *Journal of Neural Engineering*, *17*(3), 035007. https://doi.org/10.1088/1741-2552/ab8113

Baillet, S. (2017). Magnetoencephalography for brain electrophysiology and imaging. *Nature Neuroscience*, *20*(3), 327–339. https://doi.org/10.1038/nn.4504

Baldassarre, A., Ramsey, L., Rengachary, J., Zinn, K., Siegel, J. S., Metcalf, N. V., Strube, M. J., Snyder, A. Z., Corbetta, M., & Shulman, G. L. (2016). Dissociated functional connectivity profiles for motor and attention deficits in acute right-hemisphere stroke. *Brain*, *139*(7), 2024–2038. https://doi.org/10.1093/brain/aww107

Basti, A., Mur, M., Kriegeskorte, N., Pizzella, V., Marzetti, L., & Hauk, O. (2019). Analysing linear multivariate pattern transformations in neuroimaging data. *PLOS ONE*, *14*(10), e0223660. https://doi.org/10.1371/journal.pone.0223660

Basti, A., Nili, H., Hauk, O., Marzetti, L., & Henson, R. N. (2020). Multi-dimensional connectivity: A conceptual and mathematical review. *NeuroImage*, *221*, 117179. https://doi.org/10.1016/j.neuroimage.2020.117179

Basti, A., Pizzella, V., Chella, F., Romani, G. L., Nolte, G., & Marzetti, L. (2018). Disclosing large-scale directed functional connections in MEG with the multivariate phase slope index. *NeuroImage*, *175*, 161–175. https://doi.org/10.1016/j.neuroimage.2018.03.004

Bernal-Rusiel, J. L., Atienza, M., & Cantero, J. L. (2010). Determining the optimal level of smoothing in cortical thickness analysis: A hierarchical approach based on sequential statistical thresholding. *NeuroImage*, *52*(1), 158–171. https://doi.org/10.1016/j.neuroimage.2010.03.074

Betti, V., Della Penna, S., de Pasquale, F., Mantini, D., Marzetti, L., Romani, G. L., & Corbetta, M. (2013). Natural Scenes Viewing Alters the Dynamics of Functional Connectivity in the Human Brain. *Neuron*, *79*(4), 782–797. https://doi.org/10.1016/j.neuron.2013.06.022

Brancaccio, A., Tabarelli, D., Bigica, M., & Baldauf, D. (2020). Cortical source localization of sleep-stage specific oscillatory activity. *Scientific Reports*, *10*(1), 6976. https://doi.org/10.1038/s41598-020-63933-5

Brodoehl, S., Gaser, C., Dahnke, R., Witte, O. W., & Klingner, C. M. (2020). Surface-based analysis increases the specificity of cortical activation patterns and connectivity results. *Scientific Reports*, *10*(1), 5737. https://doi.org/10.1038/s41598-020-62832-z

Brookes, M. J., Hale, J. R., Zumer, J. M., Stevenson, C. M., Francis, S. T., Barnes, G. R., Owen, J. P., Morris, P. G., & Nagarajan, S. S. (2011). Measuring functional

connectivity using MEG: Methodology and comparison with fcMRI. *NeuroImage*, *56*(3), 1082–1104. https://doi.org/10.1016/j.neuroimage.2011.02.054

Bruña, R., Cuesta, P., Ramírez-Toraño, F., Suárez-Méndez, I., & Pereda, E. (2023). *The more, the merrier: Multivariate phase synchronization methods excel pairwise ones in estimating functional brain connectivity from reconstructed neural sources* (p. 2023.01.19.524740). bioRxiv. https://doi.org/10.1101/2023.01.19.524740

Bruña, R., Maestú, F., & Pereda, E. (2018). Phase locking value revisited: Teaching new tricks to an old dog. *Journal of Neural Engineering*, *15*(5), 056011. https://doi.org/10.1088/1741-2552/aacfe4

Bruña, R., & Pereda, E. (2021). Multivariate extension of phase synchronization improves the estimation of region-to-region source space functional connectivity. *Brain Multiphysics*, *2*, 100021. https://doi.org/10.1016/j.brain.2021.100021

Brunner, C., Billinger, M., Seeber, M., Mullen, T. R., & Makeig, S. (2016). Volume Conduction Influences Scalp-Based Connectivity Estimates. *Frontiers in Computational Neuroscience*, *10*. https://doi.org/10.3389/fncom.2016.00121

Calvetti, D., Pascarella, A., Pitolli, F., Somersalo, E., & Vantaggi, B. (2019). Brain Activity Mapping from MEG Data via a Hierarchical Bayesian Algorithm with Automatic Depth Weighting. *Brain Topography*, *32*(3), 363–393. https://doi.org/10.1007/s10548-018-0670-7

Capilla, A., Arana, L., García-Huéscar, M., Melcón, M., Gross, J., & Campo, P. (2022). The natural frequencies of the resting human brain: An MEG-based atlas. *NeuroImage*, *258*, 119373. https://doi.org/10.1016/j.neuroimage.2022.119373

Carter, A. R., Astafiev, S. V., Lang, C. E., Connor, L. T., Rengachary, J., Strube, M. J., Pope, D. L. W., Shulman, G. L., & Corbetta, M. (2009). Resting state inter-hemispheric

fMRI connectivity predicts performance after stroke. *Annals of Neurology*, NA-NA. https://doi.org/10.1002/ana.21905

Cekic, S., Grandjean, D., & Renaud, O. (2018). Time, frequency, and time-varying Granger-causality measures in neuroscience. *Statistics in Medicine*, *37*(11), 1910–1931. https://doi.org/10.1002/sim.7621

Chalas, N., Daube, C., Kluger, D. S., Abbasi, O., Nitsch, R., & Gross, J. (2022). Multivariate analysis of speech envelope tracking reveals coupling beyond auditory cortex. *NeuroImage*, *258*, 119395. https://doi.org/10.1016/j.neuroimage.2022.119395

Chella, F., Marzetti, L., Stenroos, M., Parkkonen, L., Ilmoniemi, R. J., Romani, G. L., & Pizzella, V. (2019). The impact of improved MEG–MRI co-registration on MEG connectivity analysis. *NeuroImage*, *197*, 354–367. https://doi.org/10.1016/j.neuroimage.2019.04.061

Chowdhury, R. A., Pellegrino, G., Aydin, Ü., Lina, J.-M., Dubeau, F., Kobayashi, E., & Grova, C. (2018). Reproducibility of EEG-MEG fusion source analysis of interictal spikes: Relevance in presurgical evaluation of epilepsy. *Human Brain Mapping*, *39*(2), 880–901. https://doi.org/10.1002/hbm.23889

Coalson, T. S., Van Essen, D. C., & Glasser, M. F. (2018). The impact of traditional neuroimaging methods on the spatial localization of cortical areas. *Proceedings of the National Academy of Sciences*, *115*(27). https://doi.org/10.1073/pnas.1801582115

Colclough, G. L., Brookes, M. J., Smith, S. M., & Woolrich, M. W. (2015). A symmetric multivariate leakage correction for MEG connectomes. *NeuroImage*, *117*, 439–448. https://doi.org/10.1016/j.neuroimage.2015.03.071

Colclough, G. L., Woolrich, M. W., Tewarie, P. K., Brookes, M. J., Quinn, A. J., & Smith, S. M. (2016). How reliable are MEG resting-state connectivity metrics? *NeuroImage*, *138*, 284–293. https://doi.org/10.1016/j.neuroimage.2016.05.070

Colenbier, N., Marino, M., Arcara, G., Frederick, B., Pellegrino, G., Marinazzo, D., & Ferrazzi, G. (2022). WHOCARES: WHOle-brain CArdiac signal REgression from highly accelerated simultaneous multi-Slice fMRI acquisitions. *Journal of Neural Engineering*, *19*(5), 056006. https://doi.org/10.1088/1741-2552/ac8bff

Colenbier, N., Sareen, E., del-Aguila Puntas, T., Griffa, A., Pellegrino, G., Mantini, D., Marinazzo, D., Arcara, G., & Amico, E. (2023). Task matters: Individual MEG signatures from naturalistic and neurophysiological brain states. *NeuroImage*, *271*, 120021. https://doi.org/10.1016/j.neuroimage.2023.120021

Cona, G., Chiossi, F., Di Tomasso, S., Pellegrino, G., Piccione, F., Bisiacchi, P., & Arcara, G. (2020). Theta and alpha oscillations as signatures of internal and external attention to delayed intentions: A magnetoencephalography (MEG) study. *NeuroImage*, *205*, 116295. https://doi.org/10.1016/j.neuroimage.2019.116295

Dale, A. M., & Sereno, M. I. (1993). Improved Localizadon of Cortical Activity by Combining EEG and MEG with MRI Cortical Surface Reconstruction: A Linear Approach. *Journal of Cognitive Neuroscience*, *5*(2), 162–176. https://doi.org/10.1162/jocn.1993.5.2.162

de Munck, J. C., Vijn, P. C., & Lopes da Silva, F. H. (1992). A random dipole model for spontaneous brain activity. *IEEE Transactions on Bio-Medical Engineering*, *39*(8), 791–804. https://doi.org/10.1109/10.148387

Desikan, R. S., Ségonne, F., Fischl, B., Quinn, B. T., Dickerson, B. C., Blacker, D., Buckner, R. L., Dale, A. M., Maguire, R. P., Hyman, B. T., Albert, M. S., & Killiany, R. J. (2006). An automated labeling system for subdividing the human cerebral cortex on MRI scans into gyral based regions of interest. *NeuroImage*, *31*(3), 968–980. https://doi.org/10.1016/j.neuroimage.2006.01.021

Dimitriadis, S. I., López, M. E., Bruña, R., Cuesta, P., Marcos, A., Maestú, F., & Pereda, E. (2018). How to Build a Functional Connectomic Biomarker for Mild Cognitive Impairment From Source Reconstructed MEG Resting-State Activity: The Combination of ROI Representation and Connectivity Estimator Matters. *Frontiers in Neuroscience*, *12*, 306. https://doi.org/10.3389/fnins.2018.00306

Eickhoff, S. B., Constable, R. T., & Yeo, B. T. T. (2018). Topographic organization of the cerebral cortex and brain cartography. *NeuroImage*, *170*, 332–347. https://doi.org/10.1016/j.neuroimage.2017.02.018

Englot, D. J., Hinkley, L. B., Kort, N. S., Imber, B. S., Mizuiri, D., Honma, S. M., Findlay, A. M., Garrett, C., Cheung, P. L., Mantle, M., Tarapore, P. E., Knowlton, R. C., Chang, E. F., Kirsch, H. E., & Nagarajan, S. S. (2015). Global and regional functional connectivity maps of neural oscillations in focal epilepsy. *Brain*, *138*(8), 2249–2262. https://doi.org/10.1093/brain/awv130

Ewald, A., Marzetti, L., Zappasodi, F., Meinecke, F. C., & Nolte, G. (2012). Estimating true brain connectivity from EEG/MEG data invariant to linear and static transformations in sensor space. *NeuroImage*, *60*(1), 476–488. https://doi.org/10.1016/j.neuroimage.2011.11.084

Fan, L., Li, H., Zhuo, J., Zhang, Y., Wang, J., Chen, L., Yang, Z., Chu, C., Xie, S., Laird, A. R., Fox, P. T., Eickhoff, S. B., Yu, C., & Jiang, T. (2016). The Human Brainnetome Atlas: A New Brain Atlas Based on Connectional Architecture. *Cerebral Cortex*, *26*(8), 3508–3526. https://doi.org/10.1093/cercor/bhw157

Farahibozorg, S.-R., Henson, R. N., & Hauk, O. (2018). Adaptive cortical parcellations for source reconstructed EEG/MEG connectomes. *NeuroImage*, *169*, 23–45. https://doi.org/10.1016/j.neuroimage.2017.09.009

Fraschini, M., Demuru, M., Crobe, A., Marrosu, F., Stam, C. J., & Hillebrand, A. (2016). The effect of epoch length on estimated EEG functional connectivity and brain network organisation. *Journal of Neural Engineering*, *13*(3), 036015. https://doi.org/10.1088/1741-2560/13/3/036015

Garcés, P., Martín-Buro, M. C., & Maestú, F. (2016). Quantifying the Test-Retest Reliability of Magnetoencephalography Resting-State Functional Connectivity. *Brain Connectivity*, *6*(6), 448–460. https://doi.org/10.1089/brain.2015.0416

Garofalo, M., Nieus, T., Massobrio, P., & Martinoia, S. (2009). Evaluation of the Performance of Information Theory-Based Methods and Cross-Correlation to Estimate the Functional Connectivity in Cortical Networks. *PLOS ONE*, *4*(8), e6482. https://doi.org/10.1371/journal.pone.0006482

Gaser, C., Dahnke, R., Thompson, P. M., Kurth, F., Luders, E., & Initiative, A. D. N. (2022). *CAT – A Computational Anatomy Toolbox for the Analysis of Structural MRI Data* (p. 2022.06.11.495736). bioRxiv. https://doi.org/10.1101/2022.06.11.495736

Gavaret, M., Badier, J.-M., Bartolomei, F., Bénar, C.-G., & Chauvel, P. (2014). MEG and EEG Sensitivity in a Case of Medial Occipital Epilepsy. *Brain Topography*, *27*(1), 192–196. https://doi.org/10.1007/s10548-013-0317-7

Geerligs, L., Cam-CAN, & Henson, R. N. (2016). Functional connectivity and structural covariance between regions of interest can be measured more accurately using multivariate distance correlation. *NeuroImage*, *135*, 16–31. https://doi.org/10.1016/j.neuroimage.2016.04.047

Gramfort, A., Luessi, M., Larson, E., Engemann, D. A., Strohmeier, D., Brodbeck, C., Parkkonen, L., & Hämäläinen, M. S. (2014). MNE software for processing MEG and EEG data. *NeuroImage*, *86*, 446–460. https://doi.org/10.1016/j.neuroimage.2013.10.027

Grova, C., Aiguabella, M., Zelmann, R., Lina, J.-M., Hall, J. A., & Kobayashi, E. (2016). Intracranial EEG potentials estimated from MEG sources: A new approach to correlate MEG and iEEG data in epilepsy: Correlation between MEG Sources and iEEG Data for Epileptic Spikes. *Human Brain Mapping*, *37*(5), 1661–1683. https://doi.org/10.1002/hbm.23127

Hagler, D. J., Saygin, A. P., & Sereno, M. I. (2006). Smoothing and cluster thresholding for cortical surface-based group analysis of fMRI data. *NeuroImage*, *33*(4), 1093–1103. https://doi.org/10.1016/j.neuroimage.2006.07.036

Hämäläinen, M. S., & Ilmoniemi, R. J. (1994). Interpreting magnetic fields of the brain: Minimum norm estimates. *Medical & Biological Engineering & Computing*, *32*(1), 35–42. https://doi.org/10.1007/BF02512476

Haufe, S., & Ewald, A. (2019). A Simulation Framework for Benchmarking EEG-Based Brain Connectivity Estimation Methodologies. *Brain Topography*, *32*(4), 625–642. https://doi.org/10.1007/s10548-016-0498-y

Haufe, S., Nikulin, V. V., Müller, K.-R., & Nolte, G. (2013). A critical assessment of connectivity measures for EEG data: A simulation study. *NeuroImage*, *64*, 120–133. https://doi.org/10.1016/j.neuroimage.2012.09.036

Hawkins, E., Akarca, D., Zhang, M., Brkić, D., Woolrich, M., Baker, K., & Astle, D. (2020). Functional network dynamics in a neurodevelopmental disorder of known genetic origin. *Human Brain Mapping*, *41*(2), 530–544. https://doi.org/10.1002/hbm.24820

He, B., Sohrabpour, A., Brown, E., & Liu, Z. (2018). Electrophysiological Source Imaging: A Noninvasive Window to Brain Dynamics. *Annual Review of Biomedical Engineering*, *20*(1), 171–196. https://doi.org/10.1146/annurev-bioeng-062117-120853

Hedrich, T., Pellegrino, G., Kobayashi, E., Lina, J.-M., & Grova, C. (2017). Comparison of the spatial resolution of source imaging techniques in high-density EEG and MEG. *Neuroimage*, *157*, 531–544.

Hillebrand, A., Barnes, G. R., Bosboom, J. L., Berendse, H. W., & Stam, C. J. (2012). Frequency-dependent functional connectivity within resting-state networks: An atlas-based MEG beamformer solution. *NeuroImage*, *59*(4), 3909–3921. https://doi.org/10.1016/j.neuroimage.2011.11.005

Hincapié, A.-S., Kujala, J., Mattout, J., Pascarella, A., Daligault, S., Delpuech, C., Mery, D., Cosmelli, D., & Jerbi, K. (2017). The impact of MEG source reconstruction method on source-space connectivity estimation: A comparison between minimum-norm solution and beamforming. *NeuroImage*, *156*, 29–42. https://doi.org/10.1016/j.neuroimage.2017.04.038

Hipp, J. F., Hawellek, D. J., Corbetta, M., Siegel, M., & Engel, A. K. (2012). Large-scale cortical correlation structure of spontaneous oscillatory activity. *Nature Neuroscience*, *15*(6), 884–890. https://doi.org/10.1038/nn.3101

Huiskamp, G., Agirre-Arrizubieta, Z., & Leijten, F. (2010). Regional Differences in the Sensitivity of MEG for Interictal Spikes in Epilepsy. *Brain Topography*, *23*(2), 159–164. https://doi.org/10.1007/s10548-010-0134-1

Irimia, A., Van Horn, J. D., & Halgren, E. (2012). Source cancellation profiles of electroencephalography and magnetoencephalography. *NeuroImage*, *59*(3), 2464–2474. https://doi.org/10.1016/j.neuroimage.2011.08.104

Korhonen, O., Palva, S., & Palva, J. M. (2014). Sparse weightings for collapsing inverse solutions to cortical parcellations optimize M/EEG source reconstruction accuracy. *Journal of Neuroscience Methods*, *226*, 147–160. https://doi.org/10.1016/j.jneumeth.2014.01.031

Kriegeskorte, N., & Bandettini, P. (2007). Analyzing for information, not activation, to exploit high-resolution fMRI. *NeuroImage*, *38*(4), 649–662. https://doi.org/10.1016/j.neuroimage.2007.02.022

Lachaux, J.-P., Rodriguez, E., Martinerie, J., & Varela, F. J. (1999). Measuring phase synchrony in brain signals. *Human Brain Mapping*, *8*(4), 194–208. https://doi.org/10.1002/(SICI)1097-0193(1999)8:4<194::AID-HBM4>3.0.CO;2-C

Lai, M., Demuru, M., Hillebrand, A., & Fraschini, M. (2018). A comparison between scalp- and source-reconstructed EEG networks. *Scientific Reports*, *8*(1), Article 1. https://doi.org/10.1038/s41598-018-30869-w

Luckhoo, H., Hale, J. R., Stokes, M. G., Nobre, A. C., Morris, P. G., Brookes, M. J., & Woolrich, M. W. (2012). Inferring task-related networks using independent component analysis in magnetoencephalography. *NeuroImage*, *62*(1), 530–541. https://doi.org/10.1016/j.neuroimage.2012.04.046

Machado, A., Cai, Z., Pellegrino, G., Marcotte, O., Vincent, T., Lina, J.-M., Kobayashi, E., & Grova, C. (2018). Optimal positioning of optodes on the scalp for personalized functional near-infrared spectroscopy investigations. *Journal of Neuroscience Methods*, *309*, 91–108. https://doi.org/10.1016/j.jneumeth.2018.08.006

Mazziotta, J., Toga, A., Evans, A., Fox, P., Lancaster, J., Zilles, K., Woods, R., Paus, T., Simpson, G., Pike, B., Holmes, C., Collins, L., Thompson, P., MacDonald, D., Iacoboni, M., Schormann, T., Amunts, K., Palomero-Gallagher, N., Geyer, S., … Mazoyer, B. (2001). A probabilistic atlas and reference system for the human brain: International Consortium for Brain Mapping (ICBM). *Philosophical Transactions of the Royal Society of London. Series B, 356*(1412), 1293–1322. https://doi.org/10.1098/rstb.2001.0915

Meier, J. D., Aflalo, T. N., Kastner, S., & Graziano, M. S. A. (2008). Complex Organization of Human Primary Motor Cortex: A High-Resolution fMRI Study. *Journal of Neurophysiology*, *100*(4), 1800–1812. https://doi.org/10.1152/jn.90531.2008

Nolte, G., Galindo-Leon, E., Li, Z., Liu, X., & Engel, A. K. (2020). Mathematical Relations Between Measures of Brain Connectivity Estimated From Electrophysiological Recordings for Gaussian Distributed Data. *Frontiers in Neuroscience*, *14*. https://www.frontiersin.org/articles/10.3389/fnins.2020.577574

Oostenveld, R., Fries, P., Maris, E., & Schoffelen, J.-M. (2011). FieldTrip: Open Source Software for Advanced Analysis of MEG, EEG, and Invasive Electrophysiological Data. *Computational Intelligence and Neuroscience*, *2011*, 1–9. https://doi.org/10.1155/2011/156869

Orlandi, J. G., Stetter, O., Soriano, J., Geisel, T., & Battaglia, D. (2014). Transfer Entropy Reconstruction and Labeling of Neuronal Connections from Simulated Calcium Imaging. *PLOS ONE*, *9*(6), e98842. https://doi.org/10.1371/journal.pone.0098842

Pagnotta, M. F., & Plomp, G. (2018). Time-varying MVAR algorithms for directed connectivity analysis: Critical comparison in simulations and benchmark EEG data. *PLOS ONE*, *13*(6), e0198846. https://doi.org/10.1371/journal.pone.0198846

Palva, J. M., Monto, S., Kulashekhar, S., & Palva, S. (2010). Neuronal synchrony reveals working memory networks and predicts individual memory capacity. *Proceedings of the National Academy of Sciences*, *107*(16), 7580–7585. https://doi.org/10.1073/pnas.0913113107

Palva, J. M., Wang, S. H., Palva, S., Zhigalov, A., Monto, S., Brookes, M. J., Schoffelen, J.-M., & Jerbi, K. (2018). Ghost interactions in MEG/EEG source space: A note of caution on inter-areal coupling measures. *NeuroImage*, *173*, 632–643. https://doi.org/10.1016/j.neuroimage.2018.02.032

Pellegrini, F., Delorme, A., Nikulin, V., & Haufe, S. (2022). *Identifying best practices for detecting inter-regional functional connectivity from EEG* (p. 2022.10.05.510753). bioRxiv. https://doi.org/10.1101/2022.10.05.510753

Pellegrino, G., Arcara, G., Cortese, A. M., Weis, L., Di Tomasso, S., Marioni, G., Masiero, S., & Piccione, F. (2019). Cortical gamma-synchrony measured with magnetoencephalography is a marker of clinical status and predicts clinical outcome in stroke survivors. *NeuroImage: Clinical*, *24*, 102092. https://doi.org/10.1016/j.nicl.2019.102092

Pellegrino, G., Hedrich, T., Chowdhury, R. A., Hall, J. A., Dubeau, F., Lina, J.-M., Kobayashi, E., & Grova, C. (2018). Clinical yield of magnetoencephalography distributed source imaging in epilepsy: A comparison with equivalent current dipole method: Distributed Magnetic Source Imaging in Epilepsy. *Human Brain Mapping*, *39*(1), 218–231. https://doi.org/10.1002/hbm.23837

Pellegrino, G., Hedrich, T., Chowdhury, R., Hall, J. A., Lina, J.-M., Dubeau, F., Kobayashi, E., & Grova, C. (2016). Source localization of the seizure onset zone from ictal EEG/MEG data: wMEM for Ictal Source Imaging. *Human Brain Mapping*, *37*(7), 2528–2546. https://doi.org/10.1002/hbm.23191

Pellegrino, G., Hedrich, T., Porras-Bettancourt, M., Lina, J., Aydin, Ü., Hall, J., Grova, C., & Kobayashi, E. (2020). Accuracy and spatial properties of distributed magnetic source imaging techniques in the investigation of focal epilepsy patients. *Human Brain Mapping*, *41*(11), 3019–3033. https://doi.org/10.1002/hbm.24994

Pellegrino, G., Machado, A., von Ellenrieder, N., Watanabe, S., Hall, J. A., Lina, J.-M., Kobayashi, E., & Grova, C. (2016). Hemodynamic Response to Interictal Epileptiform Discharges Addressed by Personalized EEG-fNIRS Recordings. *Frontiers in Neuroscience*, *10*. https://doi.org/10.3389/fnins.2016.00102

Pellegrino, G., Maran, M., Turco, C., Weis, L., Di Pino, G., Piccione, F., & Arcara, G. (2018). Bilateral Transcranial Direct Current Stimulation Reshapes Resting-State Brain Networks: A Magnetoencephalography Assessment. *Neural Plasticity*, *2018*, 1–10. https://doi.org/10.1155/2018/2782804

Pellegrino, G., Mecarelli, O., Pulitano, P., Tombini, M., Ricci, L., Lanzone, J., Brienza, M., Davassi, C., Di Lazzaro, V., & Assenza, G. (2018). Eslicarbazepine Acetate Modulates EEG Activity and Connectivity in Focal Epilepsy. *Frontiers in Neurology*, *9*, 1054. https://doi.org/10.3389/fneur.2018.01054

Pellegrino, G., Schuler, A.-L., Arcara, G., Di Pino, G., Piccione, F., & Kobayashi, E. (2022). Resting state network connectivity is attenuated by fMRI acoustic noise. *NeuroImage*, *247*, 118791. https://doi.org/10.1016/j.neuroimage.2021.118791

Pellegrino, G., Tomasevic, L., Tombini, M., Assenza, G., Bravi, M., Sterzi, S., Giacobbe, V., Zollo, L., Guglielmelli, E., Cavallo, G., Vernieri, F., & Tecchio, F. (2012). Inter-hemispheric coupling changes associate with motor improvements after robotic stroke rehabilitation. *Restorative Neurology and Neuroscience*, *30*(6), 497–510. https://doi.org/10.3233/RNN-2012-120227

Pellegrino, G., Tombini, M., Curcio, G., Campana, C., Di Pino, G., Assenza, G., Tomasevic, L., & Di Lazzaro, V. (2017). Slow Activity in Focal Epilepsy During Sleep and Wakefulness. *Clinical EEG and Neuroscience*, *48*(3), 200–208. https://doi.org/10.1177/1550059416652055

Pellegrino, G., Xu, M., Alkuwaiti, A., Porras-Bettancourt, M., Abbas, G., Lina, J.-M., Grova, C., & Kobayashi, E. (2020). Effects of Independent Component Analysis on Magnetoencephalography Source Localization in Pre-surgical Frontal Lobe Epilepsy Patients. *Frontiers in Neurology*, *11*. https://www.frontiersin.org/articles/10.3389/fneur.2020.00479

Ricci, G., Magosso, E., & Ursino, M. (2021). The Relationship between Oscillations in Brain Regions and Functional Connectivity: A Critical Analysis with the Aid of Neural Mass Models. *Brain Sciences*, *11*(4), 487. https://doi.org/10.3390/brainsci11040487

Schaefer, A., Kong, R., Gordon, E. M., Laumann, T. O., Zuo, X.-N., Holmes, A. J., Eickhoff, S. B., & Yeo, B. T. T. (2018). Local-Global Parcellation of the Human Cerebral Cortex from Intrinsic Functional Connectivity MRI. *Cerebral Cortex*, *28*(9), 3095–3114. https://doi.org/10.1093/cercor/bhx179

Schaworonkow, N., & Nikulin, V. V. (2022). Is sensor space analysis good enough? Spatial patterns as a tool for assessing spatial mixing of EEG/MEG rhythms. *NeuroImage*, *253*, 119093. https://doi.org/10.1016/j.neuroimage.2022.119093

Schnitzler, A., & Gross, J. (2005). Normal and pathological oscillatory communication in the brain. *Nature Reviews Neuroscience*, *6*(4), 285–296. https://doi.org/10.1038/nrn1650

Schuler, A.-L., Bartha-Doering, L., Jakab, A., Schwartz, E., Seidl, R., Kienast, P., Lackner, S., Langs, G., Prayer, D., & Kasprian, G. (2018). Tracing the structural origins of atypical language representation: Consequences of prenatal mirror-imaged brain asymmetries in a dizygotic twin couple. *Brain Structure and Function*, *223*, 3757–3767.

Schuler, A.-L., Ferrazzi, G., Colenbier, N., Arcara, G., Piccione, F., Ferreri, F., Marinazzo, D., & Pellegrino, G. (2022). Auditory driven gamma synchrony is associated with cortical thickness in widespread cortical areas. *NeuroImage*, *255*, 119175. https://doi.org/10.1016/j.neuroimage.2022.119175

Schuler, A.-L., & Pellegrino, G. (2021). fMRI Acoustic Noise Enhances Parasympathetic Activity in Humans. *Brain Sciences*, *11*(11), 1416. https://doi.org/10.3390/brainsci11111416

Schuler, A.-L., Tik, M., Sladky, R., Luft, C. D. B., Hoffmann, A., Woletz, M., Zioga, I., Bhattacharya, J., & Windischberger, C. (2019). Modulations in resting state networks of subcortical structures linked to creativity. *NeuroImage*, *195*, 311–319.

Siems, M., Pape, A.-A., Hipp, J. F., & Siegel, M. (2016). Measuring the cortical correlation structure of spontaneous oscillatory activity with EEG and MEG. *NeuroImage*, *129*, 345–355. https://doi.org/10.1016/j.neuroimage.2016.01.055

Sommariva, S., Sorrentino, A., Piana, M., Pizzella, V., & Marzetti, L. (2019). A comparative study of the robustness of frequency-domain connectivity measures to finite data length. *Brain Topography*, *32*, 675–695.

Tabarelli, D., Brancaccio, A., Zrenner, C., & Belardinelli, P. (2022). Functional Connectivity States of Alpha Rhythm Sources in the Human Cortex at Rest: Implications for Real-Time Brain State Dependent EEG-TMS. *Brain Sciences*, *12*(3), Article 3. https://doi.org/10.3390/brainsci12030348

Tadel, F., Baillet, S., Mosher, J. C., Pantazis, D., & Leahy, R. M. (2011). Brainstorm: A User-Friendly Application for MEG/EEG Analysis. *Computational Intelligence and Neuroscience*, *2011*, 1–13. https://doi.org/10.1155/2011/879716

Tait, L., Özkan, A., Szul, M. J., & Zhang, J. (2021). A systematic evaluation of source reconstruction of resting MEG of the human brain with a new high-resolution atlas: Performance, precision, and parcellation. *Human Brain Mapping*, *42*(14), 4685–4707. https://doi.org/10.1002/hbm.25578

Tao, J. X., Baldwin, M., Ray, A., Hawes-Ebersole, S., & Ebersole, J. S. (2007). The Impact of Cerebral Source Area and Synchrony on Recording Scalp Electroencephalography Ictal Patterns. *Epilepsia*, *48*(11), 2167–2176. https://doi.org/10.1111/j.1528-1167.2007.01224.x

Taulu, S., & Simola, J. (2006). Spatiotemporal signal space separation method for rejecting nearby interference in MEG measurements. *Physics in Medicine and Biology*, *51*(7), 1759–1768. https://doi.org/10.1088/0031-9155/51/7/008

Tesche, C. D., Uusitalo, M. A., Ilmoniemi, R. J., Huotilainen, M., Kajola, M., & Salonen, O. (1995). Signal-space projections of MEG data characterize both distributed and well-localized neuronal sources. *Electroencephalography and Clinical Neurophysiology*, *95*(3), 189–200. https://doi.org/10.1016/0013-4694(95)00064-6

Thirion, B., Varoquaux, G., Dohmatob, E., & Poline, J.-B. (2014). Which fMRI clustering gives good brain parcellations? *Frontiers in Neuroscience*, *8*. https://doi.org/10.3389/fnins.2014.00167

Thomas Yeo, B. T., Krienen, F. M., Sepulcre, J., Sabuncu, M. R., Lashkari, D., Hollinshead, M., Roffman, J. L., Smoller, J. W., Zöllei, L., Polimeni, J. R., Fischl, B., Liu, H., & Buckner, R. L. (2011). The organization of the human cerebral cortex estimated by intrinsic functional connectivity. *Journal of Neurophysiology*, *106*(3), 1125–1165. https://doi.org/10.1152/jn.00338.2011

Ursino, M., Ricci, G., & Magosso, E. (2020). Transfer Entropy as a Measure of Brain Connectivity: A Critical Analysis With the Help of Neural Mass Models. *Frontiers in Computational Neuroscience*, *14*, 45. https://doi.org/10.3389/fncom.2020.00045

Vallarino, E., Sorrentino, A., Piana, M., & Sommariva, S. (2021). The role of spectral complexity in connectivity estimation. *Axioms*, *10*(1), 35.

Van de Steen, F., Faes, L., Karahan, E., Songsiri, J., Valdes-Sosa, P. A., & Marinazzo, D. (2019). Critical Comments on EEG Sensor Space Dynamical Connectivity Analysis. *Brain Topography*, *32*(4), 643–654. https://doi.org/10.1007/s10548-016-0538-7

Varela, F., Lachaux, J.-P., Rodriguez, E., & Martinerie, J. (2001). The brainweb: Phase synchronization and large-scale integration. *Nature Reviews Neuroscience*, *2*(4), 229–239. https://doi.org/10.1038/35067550

Vicente, R., Wibral, M., Lindner, M., & Pipa, G. (2011). Transfer entropy—A model-free measure of effective connectivity for the neurosciences. *Journal of Computational Neuroscience*, *30*(1), 45–67. https://doi.org/10.1007/s10827-010-0262-3

Wang, H. E., BÃ©nar, C. G., Quilichini, P. P., Friston, K. J., Jirsa, V. K., & Bernard, C. (2014). A systematic framework for functional connectivity measures. *Frontiers in Neuroscience*, *8*. https://doi.org/10.3389/fnins.2014.00405

Wendling, F., Ansari-Asl, K., Bartolomei, F., & Senhadji, L. (2009). From EEG signals to brain connectivity: A model-based evaluation of interdependence measures. *Journal of Neuroscience Methods*, *183*(1), 9–18. https://doi.org/10.1016/j.jneumeth.2009.04.021

Wendling, F., Bartolomei, F., Bellanger, J. J., & Chauvel, P. (2002). Epileptic fast activity can be explained by a model of impaired GABAergic dendritic inhibition. *European Journal of Neuroscience*, *15*(9), 1499–1508. https://doi.org/10.1046/j.1460-9568.2002.01985.x

West, T. O., Halliday, D. M., Bressler, S. L., Farmer, S. F., & Litvak, V. (2020). Measuring directed functional connectivity using non-parametric directionality analysis: Validation and comparison with non-parametric Granger Causality. *NeuroImage*, *218*, 116796. https://doi.org/10.1016/j.neuroimage.2020.116796

Worsley, K. J., Liao, C. H., Aston, J., Petre, V., Duncan, G. H., Morales, F., & Evans, A. C. (2002). A General Statistical Analysis for fMRI Data. *NeuroImage*, *15*(1), 1–15. https://doi.org/10.1006/nimg.2001.0933

Author statement

DB, GP have conceptualised the study, analysed the data, and wrote the manuscript. SZ, GA, GP, ALS, collected the data. SS, AP developed and analysed the simulation data. JR and DM performed the clustering analysis and offered guidance on the open source scripts and data. ALS, PB, SLI, GdP, GF provided feedback on all iterations of the draft. All authors have provided feedback and input on the final version of the manuscript.

Open access resources

Code to replicate and use clustering analysis is available here: https://github.com/jrasero/connectivity-measures-clustering

MEG resting state data will be openly accessible on San Camillo Open access portal:

https://www.openaccessrepository.it/record/77043

The zipped file contains all the t-maps of the contrasts across extraction methods, ROIs, frequency bands. Maps relative to different connectivity measurements are grouped in folders. Each folder also contains the .gii file for the reference cortex surface. You may use different software to visualize these maps.

If you wish to visualize the maps with Brainstorm:

1) Go to Default Anatomy. Right Click -> Import surface. Select Group_analysis_cortex.gii.

2) Go to the Group_analysis data folder (you should create one if not present). Go to Common Files. Right Click -> File -> Import Source Maps. Select the t-maps to be visualized.

For any additional info, please get in touch with the corresponding authors.

Declaration of interest:

The authors declare that they have no known competing financial interests or personal relationships that could have appeared to influence the work reported in this manuscript.